A GRAVITATIONAL INVESTIGATION OF FRACTURE ZONES IN DEVONIAN ROCKS IN PORTIONS OF ARENAC AND BAY COUNTIES, MICHIGAN

Thesis for the Degree of M. S.

MICHIGAN STATE UNIVERSITY

John N. Roth

1965

ABSTRACT

A GRAVITATIONAL INVESTIGATION OF FRACTURE ZONES IN DEVONIAN ROCKS IN PORTIONS OF ARENAC AND BAY COUNTIES, MICHIGAN

by John N. Roth

The gravity exploration method is capable of detecting fracture zones buried at depths of 2800 feet, if the fracture zone is of sufficient width and if there is a density differential produced between the fracture zone and the surrounding country rock of 0.10 gm/cc or greater.

Three known fracture zones occurring in the Rogers City-Dundee interval of Devonian age, the North Adams, Deep River and Pinconning, are studied by the gravity method using graphical, statistical and analytical techniques of interpretation. The characteristics of the fracture zones and their associated anomalies are studied, and the optimum methods of isolation are discussed.

Theoretical calculations indicate that the anomalies associated with the fracture zones are positive and may have a magnitude as great as 0.27 mgals. The source of the fracture zone anomalies is lateral variations in the density of the porous dolomitized fracture zone and the surrounding tight limestone.

The North Adams fracture zone has a positive anomaly associated with it that has a mean amplitude of 0.15 mgals. The Deep River and Pinconning fractures do not have anomalies correlative with them.

There are negative anomalies due to buried bedrock valleys that are capable of masking the fracture zone anomalies. In areas where the bedrock topography is known, the effects of the bedrock valleys can be determined and eliminated from the interpretation. Theoretical calculations using the configuration of the bedrock valleys show that the valleys can produce gravity effects equal to those observed.

There is no correlation, either positive or negative, between the gravity maps and the Paleozoic structures, that are present in the area.

Graphical and statistical methods isolate the anomalies associated with the fracture zones.

A limited study of the application of upward continuation, downward continuation, and second derivative methods to isolating fracture zone anomalies indicates that these techniques have no advantage over the statistical methods in this investigation.

A GRAVITATIONAL INVESTIGATION OF FRACTURE ZONES IN DEVONIAN ROCKS IN PORTIONS OF ARENAC AND BAY COUNTIES, MICHIGAN

By

John N. Roth

A THESIS

Submitted to
Michigan State University
in partial fulfillment of the requirements

MASTER OF SCIENCE

Department of Geology

1965

ACKNOWLEDGMENTS

The author wishes to express his sincere thanks to the following individuals and organizations.

To Dr. W. J. Hinze for his sincere interest, guidance, and helpful criticism during the study and preparation of this manuscript.

To Dr. C. E. Prouty for reviewing the manuscript and for his helpful suggestions.

To Mr. C. K. Dean for making available the data and well samples for this study, and for his aid during the study.

To Mr. D. W. Merritt for his assistance in preparing the data for the computer and for the use of several of his programs.

To Michigan State University for free use of the C.D.C. 3600 computer.

TABLE OF CONTENTS

TABLE OF CONTENTS

LIST OF FIGURES

CHAPTER I

INTRODUCTION

There are several fracture zones in the central area of the Michigan Basin that are important petroleum reservoirs. It has been extremely difficult to locate these zones of porous dolomite. The masking of the bedrock by the glacial drift and the depths to the Devonian reservoir rocks near the center of the Basin have been handicaps to exploration. Since the late 1930's and early 1940's, when these zones were first being discovered, the only successful method of locating them has been by wildcat drilling.

To date, there has been no method described for delineating these features by the gravity exploration method. It is therefore the purpose of this study to determine if known fracture zones give rise to gravity anomalies, and if so, what are the optimum methods for isolating the anomalies.

The area of investigation located in the southwest portion of Arenac County and the northern portion of Bay County, Michigan, has been penetrated by a large number of wells. The majority of them are located in the

northern half of the study area (Arenac County). The geology is known quite well and is used with the geophysics to arrive at an overall geological and geophysical interpretation of the area.

The southern half of the area (Bay County) has only a small number of drilled wells. They are concentrated in two fields, the Mt. Forest and Pinconning. There are also a few scattered test wells in the area. Due to lack of geological control, this area is interpreted with the methods found best for interpreting the northern half of the study area.

CHAPTER II

GEOGRAPHY OF THE AREA

The area under investigation, shown by the diagonal parallel lines in Figure 1, is located in Arenac and Bay counties, Michigan. Townships 16 and 17 north, Range 4 east comprise the majority of the area in Bay County. Parts of Townships 15, 16, 17, and 18 north, Range 3 east and Township 15 north, Range 4 east are also included. This portion of the study area is referred to as the Pinconning area or the southern half of the study area.

In Arenac County, Townships 18 and 19 north, Range 3 east, cover most of the area. Parts of Townships 18 and 19 north, Range 5 east, and three sections in Township 20 north, Range 4 east, make up the remainder of the study area in Arenac County. This area is referred as the Deep River or northern half of the study area.

The area as a whole is a flat glacial lake bed. The area slopes in a southeast direction toward Saginaw Bay, and Lake Huron. The only relief encountered is that of the major river beds in the area. They are the Rifle River and three branches of the Pine River in the northern half of the study area, and the Pinconning and Kawkawlin Rivers in the southern half of the study area.

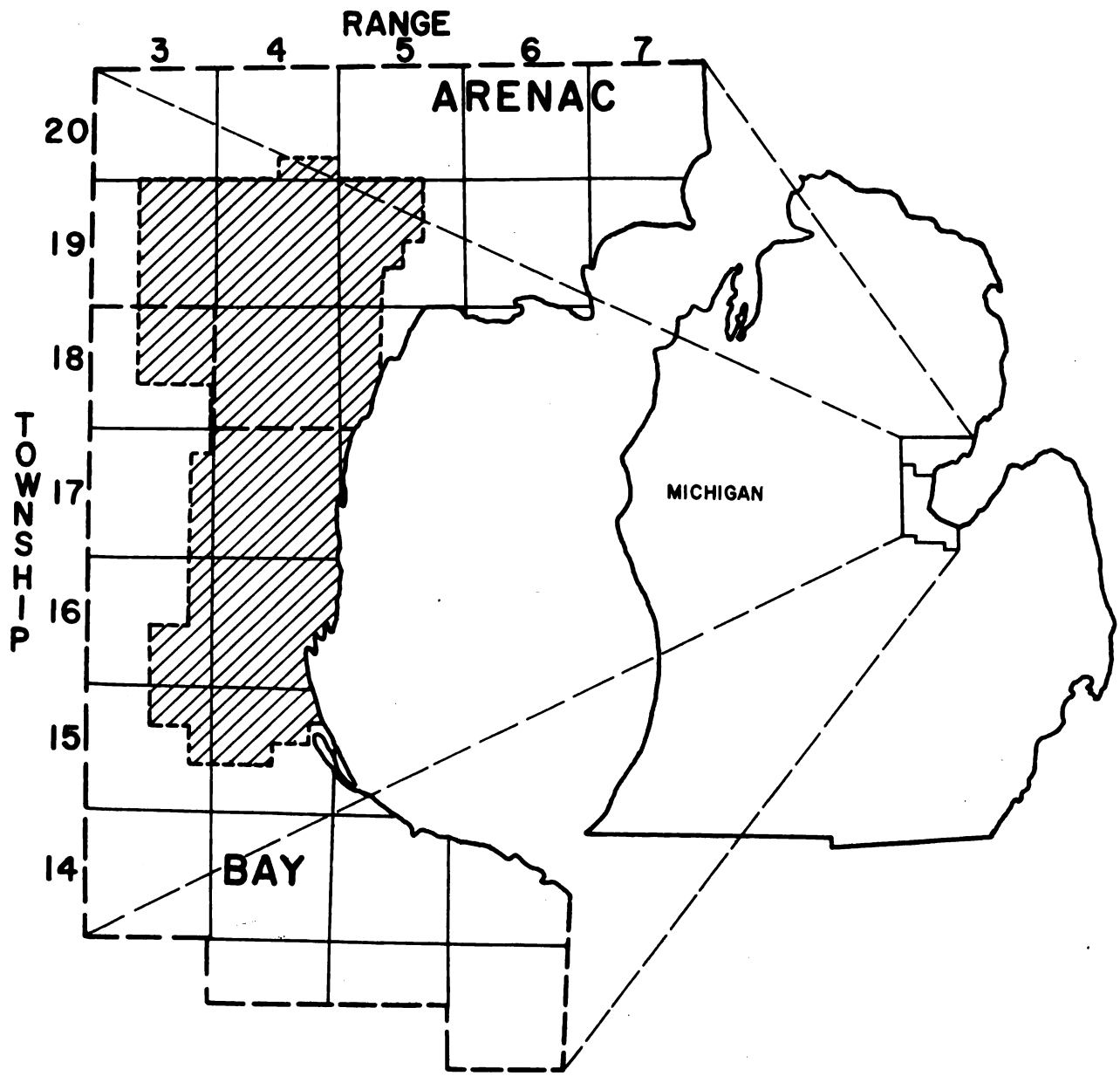

AREA OF INVESTIGATION

FIGURE 1

Geographically the area lies wholly within a physiographic subdivision known as the Saginaw Lowland (Newcombe, 1933).

Of major interest to the investigation are the known oil fields in the area. Their names and locations are shown in Figure 2. The largest is the Deep River Field. It is located in the northern half of Township 19 north, Range 4 east, and extends for 5 1/4 miles in a northwest direction. It is about 1 1/4 miles northeast of the town of Sterling and approximately 30 miles north of Bay City, Michigan. The North and South Adams Fields are located in Township 19 north, Range 3 east. The North Adams Field trends northeast for three miles, approximately at right angles to the Deep River Field. The South Adams Field is approximately one mile east of the southern end of the North Adams field. One mile south of the South Adams field is the Adams Detroit River Field.

Another field of importance in the northern half of the study area is the Sterling Field. It is located one half mile south of the Deep River Field and produces from the same structure.

There are two fields of importance in the Pinconning portion of the study area. These are the Pinconning and Mt. Forest Fields. The Pinconning Field is located in the southeast quarter of Township 17 north, Range 4 east. It extends about two miles in a northeast direction and is

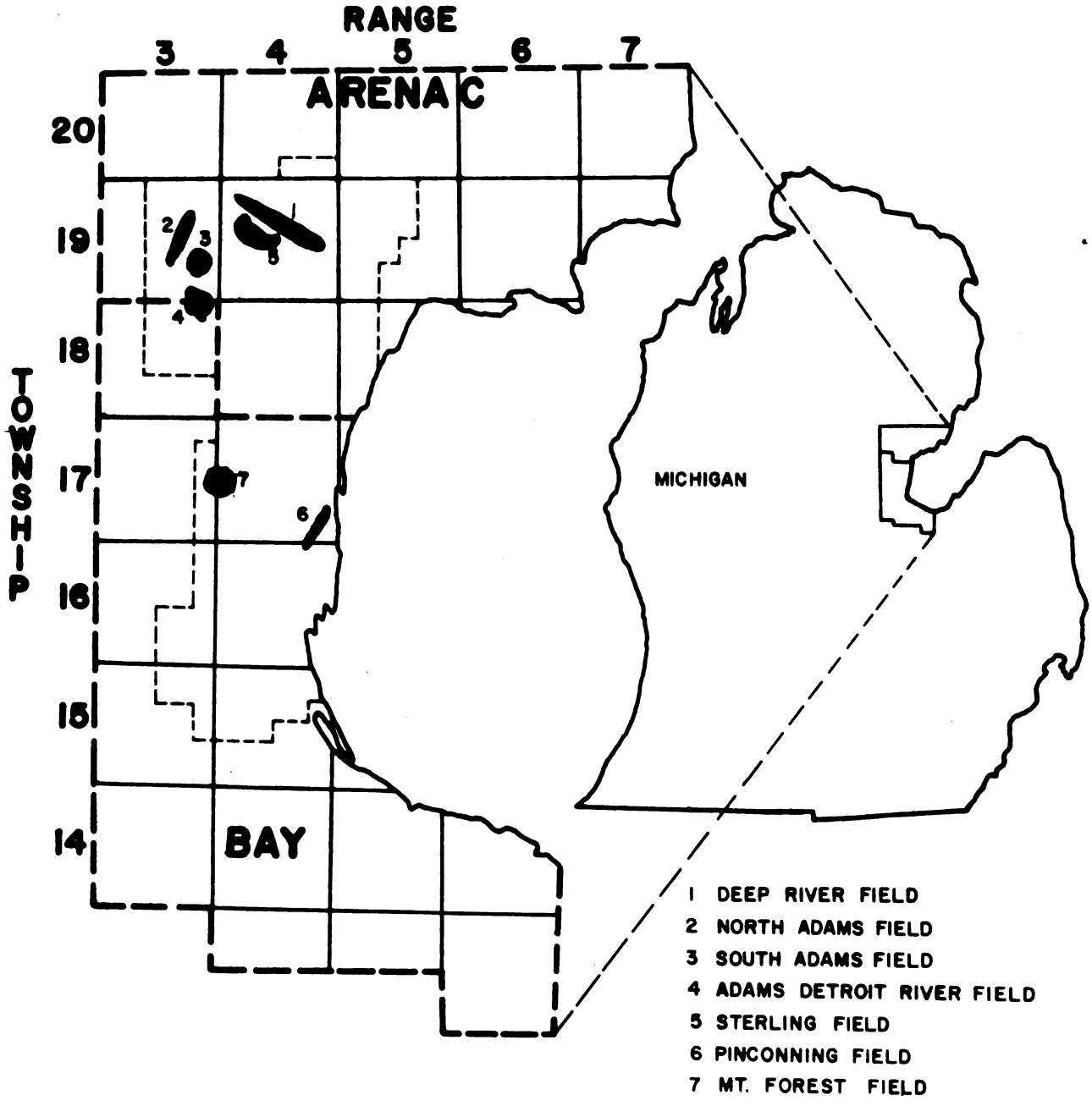

LOCATION OF OIL FIELDS

FIGURE 2

only 1000 feet wide at its broadest point. The Mt. Forest Field is located on the border line of Township 17 north, Range 3 and 4 east.

There are also four producing wells located halfway between the Pinconning and Mt. Forest fields. The production is in section 29 of Township 17 north, Range 4 east. It is named the Lucht Field and is of minor importance, therefore, it is not shown in Figure 2.

CHAPTER III

GEOLOGY OF THE AREA

Stratigraphy of the Area

The area under investigation is covered with glacial drift ranging in thickness from 20 to nearly 300 feet in some areas. The drift consists essentially of glacial-lake clays and some sand beds.

The Saginaw Formation lies directly below the glacial drift in all of the southern portion of the survey area. The Saginaw Formation of early (Pottsville) Pennsylvanian age consists mostly of clastic sediments. In the northern portion of the area, the Parma Sandstone, Michigan Formation, or the Bayport Limestone may be encountered just below the drift.

The Parma Sandstone is white and clean and lies unconformably over the brown Bayport Limestone. A gray shale called the Michigan Formation lies below the Bayport. The Michigan also contains some dolomite, limestone, gypsum and sandstone. The Marshall Sandstone and its member, the Napoleon Sandstone, lies unconformably below the Michigan Formation. It is a white to gray sandstone, and is calcareous in its lower part.

Below the Marshall is the Coldwater Shale of early Mississippian age. It also contains beds of dolomite, siltstone and sandstone.

The Sunbury Shale which is thin and black lies below the Coldwater. The Sunbury is of questionable age, being assigned either to the Mississippian or Devonian systems. It averages only 25 feet in thickness and is similar to the earlier Antrim Shale except that it is more carbonaceous. It produces gas at one locality in the Deep River area. In Michigan, the Berea is assigned to either the Mississippian or Devonian systems. In other areas it is assigned to the Mississippian system. The bedford Shale lies below the Berea and is of late Devonian age. The Antrim Shale of late Devonian time (Chautauquan series), lies below the Bedford and is similar in nature.

Beneath the Antrim lies the thick Traverse group, primarily middle Devonian in age. Its formations are generally undivided in the subsurface. They are mainly gray shaley limestones and shales. The lowest formation in the Traverse is the Bell Shale. It varies in thickness and has led some geologists to believe it rests unconformably above the Rogers City-Dundee interval. It is a soft fossiliferous gray shale, usually thin (not thicker than 80 feet), and makes a good marker bed.

The Rogers City-Dundee interval is an important target depth for oil in Michigan. Eighty-four per cent

of Michigan's oil up to 1945 had been produced from these formations. The Rogers City-Dundee interval is the major oil producing zone of all the large fields in the survey area. It is primarily a limestone, but locally it has been altered to a dolomite. The producing zone is usually within the top 10-15 feet of the interval. The interval is described as one unit on most well logs of the area, and is usually referred to as the Dundee, but the units have been described separately by Ehlers (1938).

The Rogers City Formation varies from 75 to 100 feet in thickness in the Pinconning Field and from 100 to 125 feet in the Deep River Field. The Rogers City has its thickest point in the entire state in Arenac County. It is predominately a brownish limestone in the eastern part of the state, but locally has been altered to dolomite in the Deep River, North Adams, and Pinconning Fields.

The Dundee below the Rogers City is productive in many parts of the state, but in the study area production is mostly from the Rogers City. It varies in thickness from about 250-350 feet and also has its thickest point in Arenac County. It is a massive buff to light brown limestone, with areas of dolomitic limestone, and dolomite.

A few wells in the area have penetrated the entire thickness of the Rogers City-Dundee interval to the Detroit River which lies conformably below. It consists of alternating beds of dolomite, limestone, sandstone, salt, and

gypsum. It is not of importance in this study, so it will not be discussed in detail.

Figure 3 is a stratigraphic chart showing the various above mentioned rock units, their relative positions and ages.

Regional Geology

The area under investigation lies just north and east of the center of the roughly circular Michigan structural basin. The Basin includes the Southern Peninsula of Michigan and extends outward into the surrounding states and Canada. Outcrops of Precambrian rocks limit the Basin to the north. The limiting features on the south are the Findlay and Kankakee Arches of northwestern Ohio and northern Indiana, respectively. To the east, the limiting feature is the Algonquin axis running northeast through Ontario. The bordering feature to the west is the Wisconsin Arch in central Wisconsin.

The Winconsin Arch was present in Precambrian time, and the north and northeast boundaries also were fixed by the beginning of Cambrian time (Ver Wiebe, 1952). The Michigan Basin was probably part of a larger basin in Cambrian time, one that had its greatest development in Illinois. The evidence for this is the thinning of the Cambrian rocks in the Michigan Basin to the north. The eastern border of the Basin is suggested by the thinning of beds on the Ontario arch (Ver Wiebe, 1952).

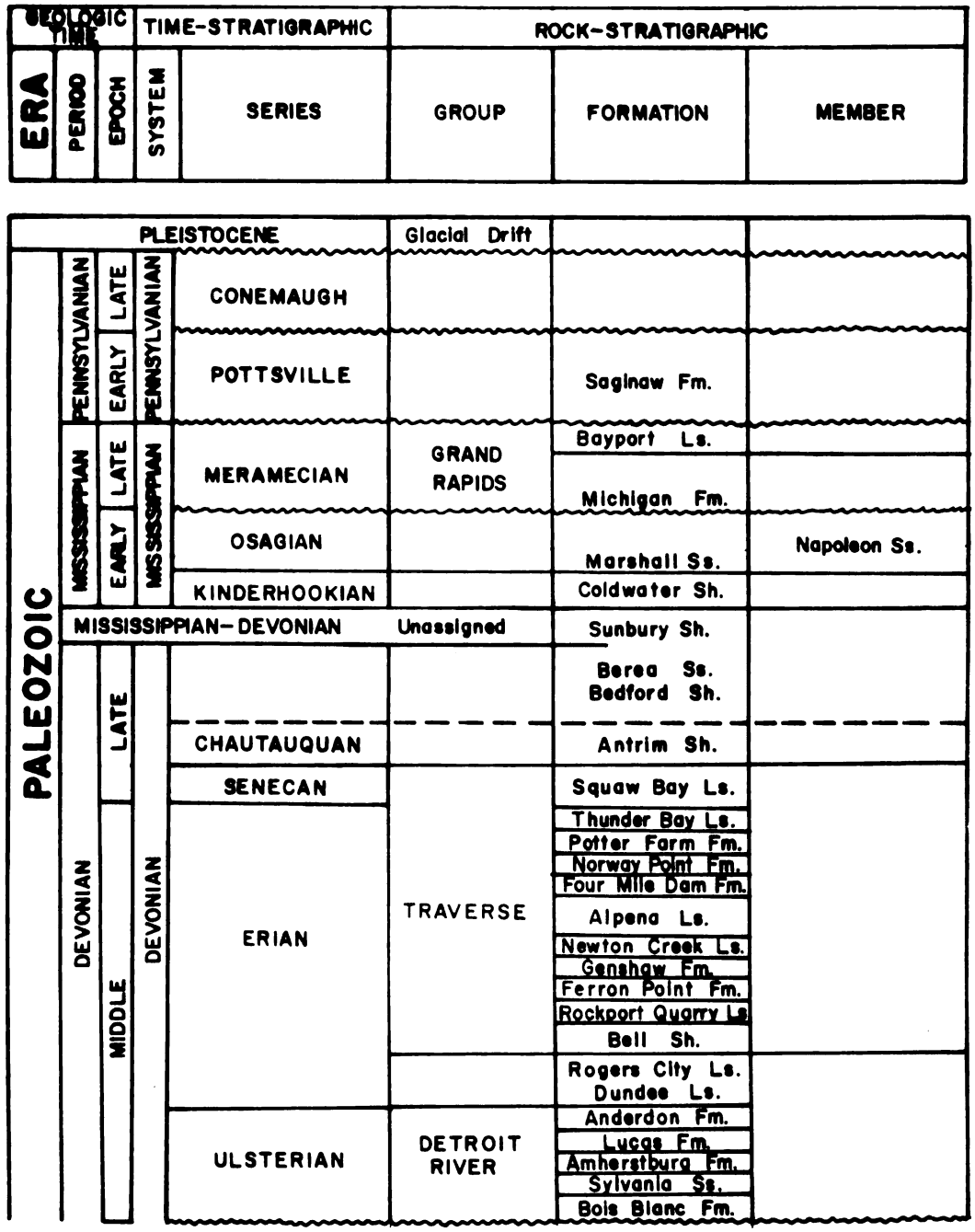

STRATIGRAPHIC SUCCESSION OF MICHIGAN

FROM RECENT THROUGH MAJOR PRODUCING ZONES OF THE AREA

(MODIFIED after MICHIGAN DEPARTMENT OF CONSERVATION, 1964)

FIGURE 3

Most likely, the Kankakee and Findlay Arches were developed in Ordovician time. These changes in structural character are inferred by the great unconformity between the Ordovician-Black River rocks and the underlying strata, and the slight thinning of these rocks over the Kankakee Arch suggests its development at this time (Ver Wiebe, 1952).

The thickening of the above mentioned sediments toward the center of the Basin, suggests that it was subsiding then. Subsidence continued in early and middle Silurian time, but the Basin appears to have tilted as well. This is evidenced by the Cataract and Niagara rocks thickening to the north (Ver Wiebe, 1952).

There was rapid subsidence in late Silurian time as suggested by the thick Salina group. The Salina has a great amount of salt within it, indicating an arid climate.

Subsidence continued through Devonian time but the center of the basin shifted some 50 miles eastward. Together, the Silurian and Devonian periods account for the majority of subsidence in the Michigan Basin, amounting to more than 7000 feet. Rocks of Silurian age crop out along the northern edges of the Findlay and Kankakee Arches. Rocks of Ordovician age crop out to the west and northwest through Wisconsin and the Northern Peninsula of Michigan. In southwest Ontario, rocks of Devonian age are at the surface. Further northeast along the Algonquin axis rocks of Ordovician and Silurian age are exposed.

As one travels from the outcrop areas around the margin of the Basin, the beds occur in rings and become progressively younger toward the center of the Basin, where rocks of Pennsylvanian age generally are beneath the glacial drift.

Within the Basin itself, definite structural trends are noted. The dominant trend near the center of the Basin is northwest-southeast, as exhibited by the largest structure in the Basin, the Howell Anticline. Figure 4 is a map of the bedrock geology of the study area. In the northern portion of the area, northwest-southeast trends are also noted. Around the margins of the basin, other trends are noted.

In the southwestern portion of the Basin, there appears to be no dominant structural trend. According to Ver Wiebe, this portion of the Basin shows many local depressions, which he attributes to a collapse phenomena due to leaching of the salt of the Salina group. His evidence for this is the abnormal rapid thinning of salt in that part of the Basin.

Local Structure and Geology

Figure 4 shows a northwest-southeast trending anticline in the center of the northern half of the area. The older Michigan formation surrounded by the younger Pennsylvanian Parma Sandstone of the Saginaw group indicate its presence at the bedrock surface. This is a reflection

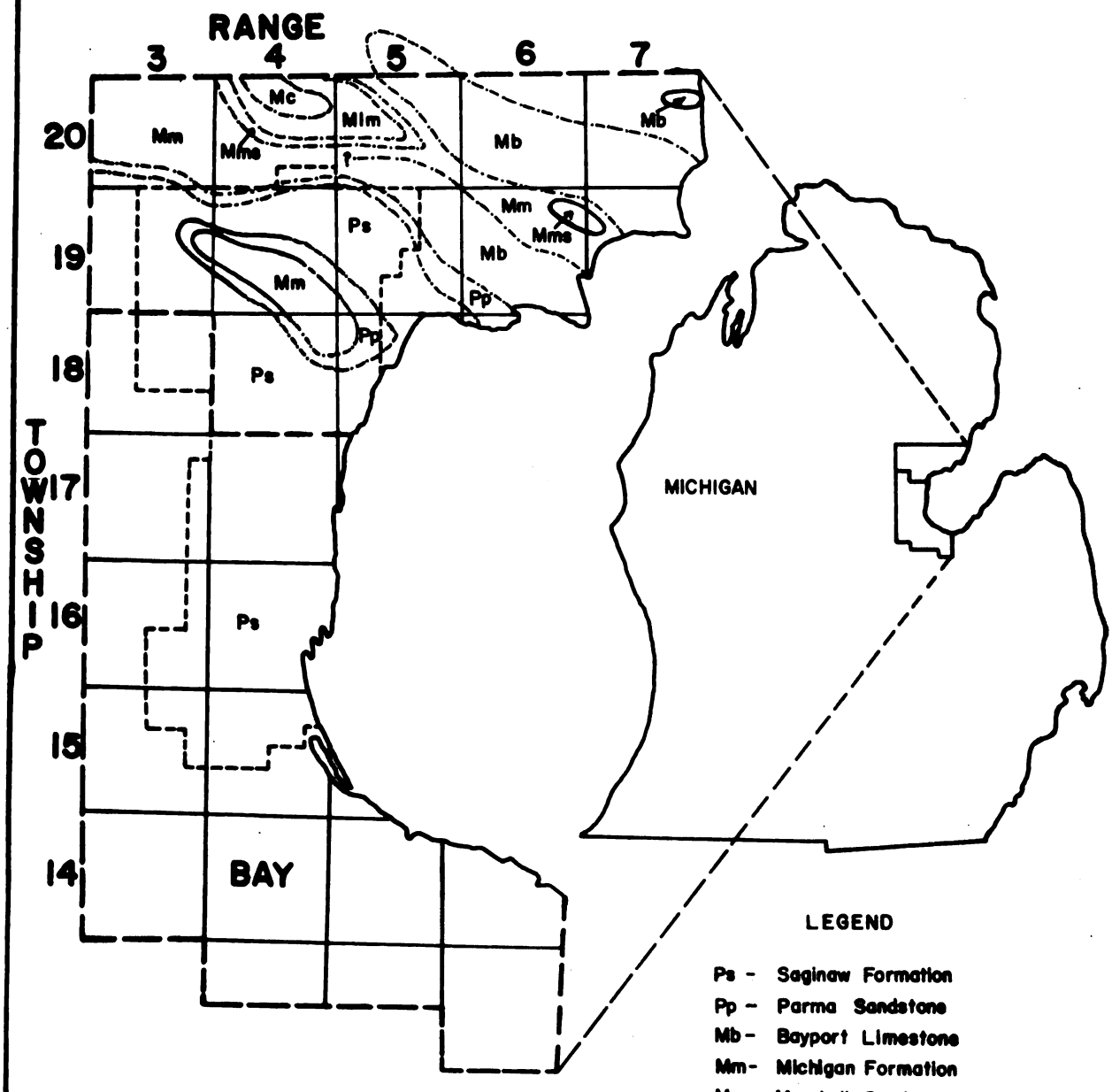

BEDROCK GEOLOGY OF THE AREA

(after MARTIN, 1936)

FIGURE 4

of the deeper feature responsible for some of the oil accumulation in that area.

At the very top of the figure, another similar feature can be seen. It is a more pronounced feature as shown by the older Mississippian Coldwater Shale cropping out in the northern half of Township 20 north, Range 4 east.

An interesting fact, although not pertinent to this study, is the fact that Figure 4 is part of a bedrock geology map published in 1936. The fields on the southern most of the two trends were not discovered until after 1936.

Figure 5 is a structure contour map on the base of the Traverse group, covering the Deep River area in Arenac County. Again local northwest-southeast structural trends are noted. The Deep River Anticline, covering most of the northwest quarter and central portion of Township 19 north, Range 4 east, is the largest feature in the area. Although the closure on a major anticline in the central area of the Michigan Basin, such as this one, is often greater than 100 feet, oil production is generally obtained from the upper 40 to 60 feet. In fields where porosity is due to dolomitization, production may be found on the flanks of the structure and not on the crest. The Deep River Field actually was found after the development of the Deep River gas field had determined the presence of

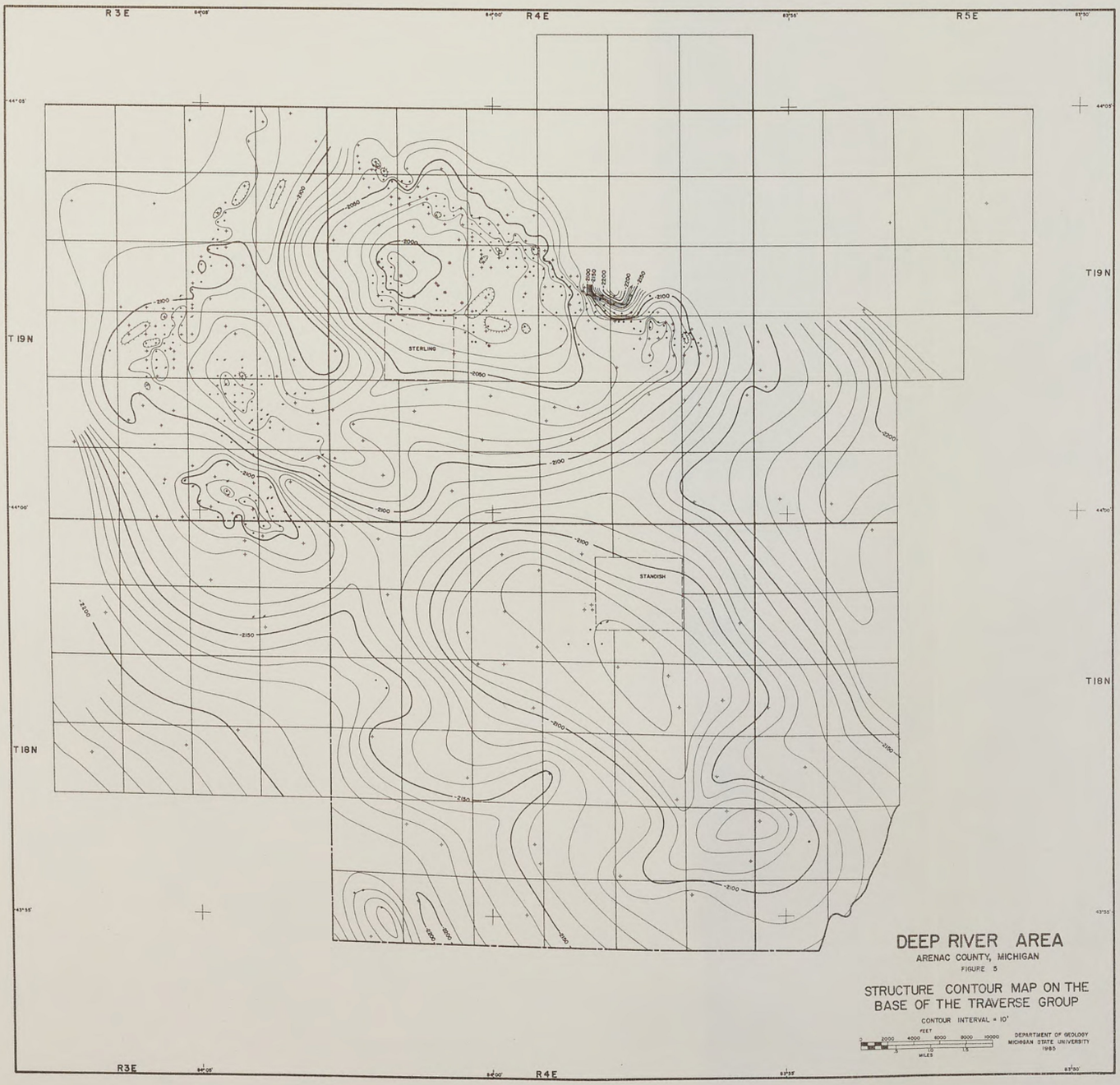
R3E
R4E
R5E
T19N
T18N
STERLING
STANDISH
-2100
-2150
-2200
-2050
-2000
-1950
-1900
-2250
-2300
DEEP RIVER AREA
ARENAC COUNTY, MICHIGAN
FIGURE 5
STRUCTURE CONTOUR MAP ON THE BASE OF THE TRAVERSE GROUP
CONTOUR INTERVAL = 10'
FEET
0 2000 4000 6000 8000 10000
0 1 2 MILES
DEPARTMENT OF GEOLOGY
MICHIGAN STATE UNIVERSITY
1985

an anticline (Landes, 1956). The discovery well was the Werblo well in the south 1/2 of the NW 1/4, NW 1/4 of section 1. The well was drilled off the dome and some 50 feet structurally lower. Its total depth is 2846 feet, penetrating 8 feet of the Rogers City Dolomite. Had the operator not drilled some 1200 feet below the base of the Berea gas zone, the field might not have been discovered. The Deep River oil Field is parallel to the regional trends of the area, but its production is due to a fracture zone with porosity due to dolomitization.

The North and South Adams Fields are located on a northwest-southeast trending nose. The North Adams Field also is due to porosity by dolomitization. The South Adams Field is structurally high on the nose.

The Adams Detroit River Field is located on a small anticline in the extreme southeast portion of Township 19 north, Range 3 east.

A small field, the Standish, located at the southwest corner of the City of Standish is also on a northwest-southeast trending structural high. The closure here is not nearly as great as that of the Deep River Anticline. This may account for the lower amount of production of oil.

In the extreme southwest corner of Figure 5, three wells have been drilled and are producing. No name has been given to this field as far as the writer knows. It again, is situated on a structure conforming to the regional trend.

Figure 6 is a structure contour map on the base of the Traverse group. The contour interval is 10 feet. The map covers the southern half of the study area or the Pinconning area. The same structural trends are noted again. The Mt. Forest Field is located on a northwest-southeast trending high running through the southern half of Township 17 north, Range 4 east.

The small field located in section 29 also is on a northwest-southeast trending high. It is paralleled in sections 27 and 28 by a similarly aligned trough. A saddle separates this small field from the Mt. Forest Field.

The Pinconning Field located in the extreme southeast portion of Township 17 north, Range 4 east, cuts perpendicularly across the trends of the area. A fault shown in the southern end of the field may well run the entire length, but is not shown due to lack of control.

A large structural trough shown by dashed contour lines is located in the northwest corner of Township 16 north, Range 4 east. The contours are dashed in this area due to the sparseness of wells.

The extreme southern portion of the map shows the start of another northwest-southeast trending high. If this map were continued a few miles south, it would include, on this high, the large Kawkawlin oil field.

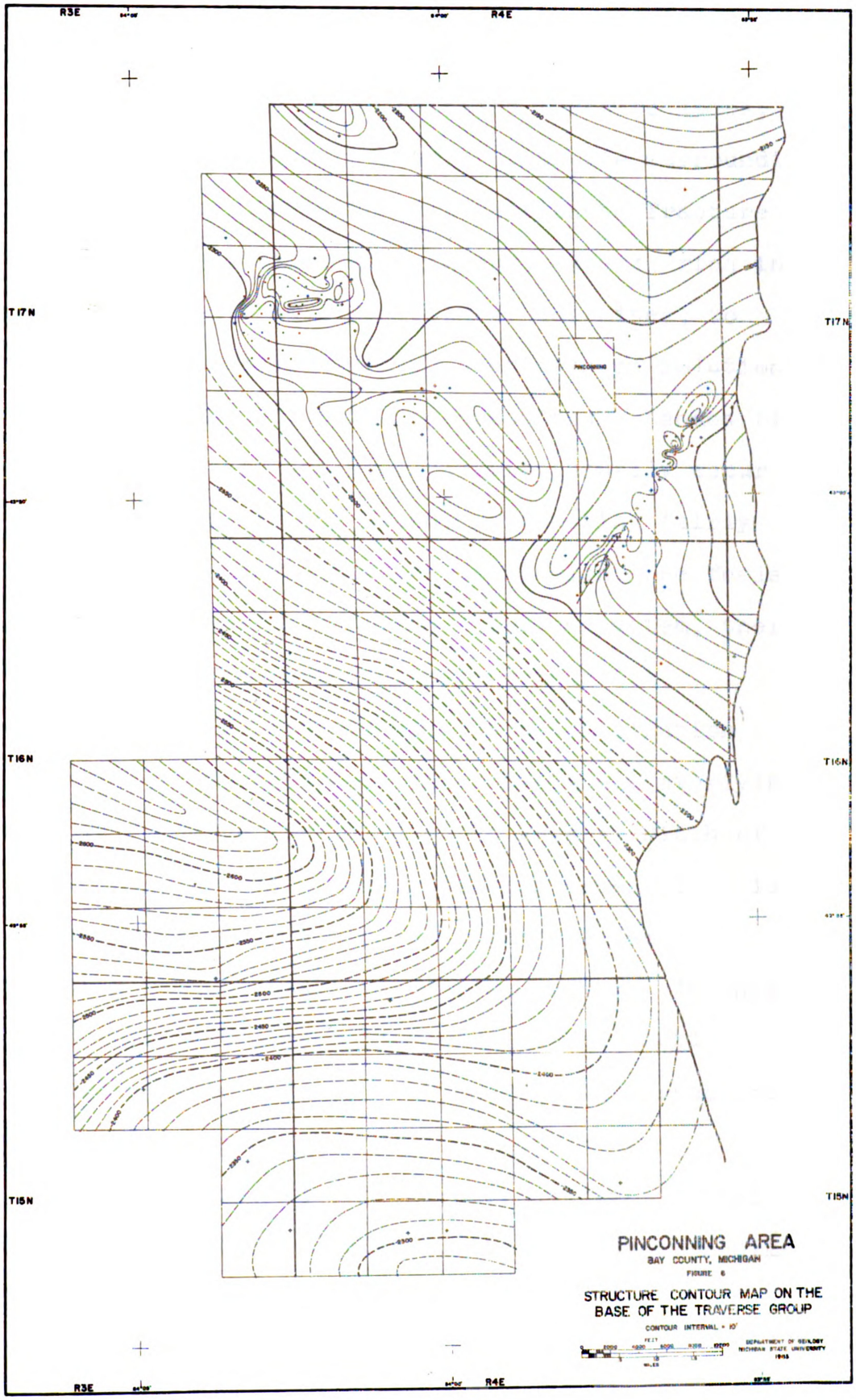
R3E
R4E
T17N
T16N
T15N
PINCONNING
PINCONNING AREA
BAY COUNTY, MICHIGAN
FIGURE 6
STRUCTURE CONTOUR MAP ON THE
BASE OF THE TRAVERSE GROUP
CONTOUR INTERVAL = 10'
DEPARTMENT OF GEOLOGY
MICHIGAN STATE UNIVERSITY
1965

Porosity by Dolomitization

Oil has accumulated in the Deep River, North Adams and Pinconning Fields in dolomitized fracture zones, where the porosity is much greater than the surrounding tight limestones. It is thought that these fracture zones have allowed circulating ground waters, rich in magnesia, derived from older primary dolomites, to ascend to the surface. Through a process of solution and precipatation, the dolomite was deposited. Landes (1946) states that solution and precipitation usually occur at the same rate, but if the waters were moving fairly rapidly, solution may exceed precipitation. He feels that the waters were part of an artesian system, therefore, assumed to be moving fairly rapidly.

Landes (1958) states that the dolomitization porosity may be younger than the immediately overlying rock. His evidence for this is the greater width of porosity near the top of the producing zone. This is due to the Bell Shale acting as a partial dam, restricting the vertically ascending waters. In this case the water would move laterally at the contact of the producing zone and the Bell shale, thus producing a wider zone of porosity.

An alternative theory, also by Landes, is that dolomitization occurred prior to the Bell Shale sedimentation. The greater width of dolomite at the top of the

producing Rogers City formation is due to the greater development of weathering porosity, on either side of the major fracture, at that level.

No well in any of the three fields was even drilled completely through the fracture zone. This tends to disagree with Landes' wider zone of porosity at the top of the formation, but supports the fact that the fractures are nearly vertical. Since no well has ever penetrated the fracture zone, the depth to its bottom can only be estimated.

Relation to Fracture Zones to Regional Geology

The structural trends and fractures in the study area have been explained, in terms of the regional geology, by several different theories.

Lockett (1947) states that during the Paleozoic era, three sides of the Michigan structural basin remained more or less stationary while the southeast end continued to subside in the Chatham Sag area. He further states, that under these conditions, a system of fractures or lines of weakness developed in the basal complex, radiating from the unsupported end. These fractures trending northwest-southeast have thus developed from simple subsidence.

Pirtle (1932) states that there is some indication of cross folding near the center of the basin. The forces that caused these folds, perpendicular to the general

structural trend, were less intense. This may account for the fact that the northeast-southwest trending North Adams and Pinconning fractures are less developed than the Deep River fracture zone.

Pirtle attributes the major trends to regional diastrophism which was active during several periods but was probably most intense during the Mississippian period.

Lockett states that it seems highly improbable that deformational stresses could have been transmitted through the basin even if it had been appreciably compressed. Orogenic forces imply mountain building activity. He further states, "anticlinal folds with relief of approximately 1000 feet, such as the Howell Anticline, when considered in their true relation to the extent of the basin seem hardly of sufficient proportion to warrant the assumption of crumpling orogenic forces to account for their formation."

CHAPTER IV

REDUCTION OF DATA

Introduction

Observed gravity values must be corrected for the effect of station elevation, latitude, and terrain, before they are useful in geophysical studies. These corrections are applied to each station and the resulting value is called the Bouguer gravity anomaly.

The complete Bouguer gravity anomaly was calculated on a digital computer according to the following formula:

$$G_{bga} = g_o - g_l + g_e - g_m + g_t$$

where

G_{bga} = complete Bouguer gravity anomaly

g_o = observed gravity

g_l = latitude correction

g_e = free-air correction

g_m = mass correction

g_t = terrain correction

Observed Gravity

The observed gravity values were measured by a contract geophysical crew and made available for this study. Briefly, the observed gravity is calculated as follows:

The meter readings collected in the field are corrected for time variations or drift, and the values are multiplied by the calibration constant of the meter. The amount of drift is determined from graphs of base-check readings.

Latitude Correction

The latitude correction takes into account the increase in gravity from the equator to the poles. In this case latitude corrections were made from latitude 43°40', which was arbitrarily selected as the base latitude. Latitude corrections are made from the base latitude by multiplying the distance of each station from this latitude by a constant, K. Nettleton (1940) determined K to be 1.307 sin 2θ mgal per mile, where θ is the mean latitude of the survey. In this study the mean latitude is 43°50', and K was determined to be 0.0002474 mgals per foot.

Free-Air Correction

The free-air correction takes into account the decrease in gravity with an increase in elevation. This correction was calculated by multiplying the vertical gradient of gravity, 0.09406 mgals per foot, by the elevation differential between the gravity station and the datum.

Mass Correction

The mass correction takes into account the increase in gravity due to the attraction of material between the datum and the individual stations. The formula to determine the mass correction is $0.01276\rho h$ mgals per foot, where ρ = density (2.1 gm/cc), and h = the elevation difference between individual stations and the datum. The datum to which the gravity values were reduced is 650.0 feet, approximately the mean elevation of the survey area.

The determination of the correct density of the near surface material is extremely important. In this area a density of 2.1 gm/cc was employed. This value was determined by using the Nettleton density profile method. Klasner (1964) determined a density of 2.15 gm/cc for the near surface material in southwestern Michigan, and Servos (1965) determined a density of 2.1 gm/cc for material near the surface in southeastern Michigan.

Terrain Correction

The relief in the area was low enough so that no terrain corrections were needed. Where local variations, such as stream beds were encountered, the stations were placed far enough away so that the effect of the feature was negligible upon the gravity reading.

CHAPTER V

ACCURACY OF BOUGUER REDUCTIONS

There are several factors that cause error in the computed Bouguer gravity anomaly. These are:

1. Errors in observed gravity
2. Errors in elevation
3. Errors in latitude
4. Errors in the assumed density of near surface material

An estimate of the accuracy of the gravimeter readings and drift control can be obtained by re-observing previously occupied stations. The standard deviation for these repeated gravity observations is 0.04 mgals.

Errors in station elevation can cause considerable error in the Bouguer gravity anomaly. Errors can be determined by closing survey elevation loops. The allowable error of closure in this case was 0.5 feet. By combining the free-air and mass effects, an error of 0.034 mgals would occur for a station 0.5 feet in error at a density of 2.1 gm/cc.

Errors in the latitude correction depend on the accuracy of the latitude measurements. Latitude corrections were made to an accuracy of 200 feet or better on the base maps used in this study. An error in

latitude of 200 feet would result in an error of 0.049 mgals. at 0.0002474 mgals per foot.

An incorrectly chosen density value of 0.1 gm/cc with a change in elevation between two stations of 20 feet will cause an error of 0.025 mgal. The formula for calculating this error is:

$$\text{Error} = 0.00128\rho h$$

where

0.00128 = magnitude of error in mgals per foot for each 0.1 gm/cc error in density

ρ = error in density in units of 0.1 gm./c.c.

h = maximum relief in feet

In areas of no relief an error in choosing the density would result in a constant error for each station and would not affect the results of the survey.

A combination of possible errors in observed gravity, elevation, mass, and latitude corrections could result in a maximum error of 0.15 mgals. It is however, unlikely that the signs of each possible error would coincide at any station.

CHAPTER VI

REGIONAL GRAVITY ANOMALY

The Bouguer gravity anomaly maps shown in Figures 7 and 8 show the results of combining the previously mentioned data reductions to each gravity station. The two maps show a decrease in regional gravity from 78.50 mgals. in the south to 66.50 mgals. in the north. The northern portion of Figure 8 and the southern portion of Figure 7 show the gravity decreasing in a regular manner. Two large anomalous areas that interrupt the regional picture are readily apparent. One is the complex gravity in the northwest portion of Figure 7, and the other area occupies the southern portion of Figure 8.

These maps show excellent agreement with Figure 9, the regional gravity map of Michigan (Hinze, 1963). The area lies partially on the southeast flank of a regional gravity minimum that has a closure of 6 mgals. The southern portion of the study area lies in an area of slightly complicated regional gravity.

Besides the two large anomalous areas, there are several other smaller anomalous areas that can be seen in Figures 7 and 8.

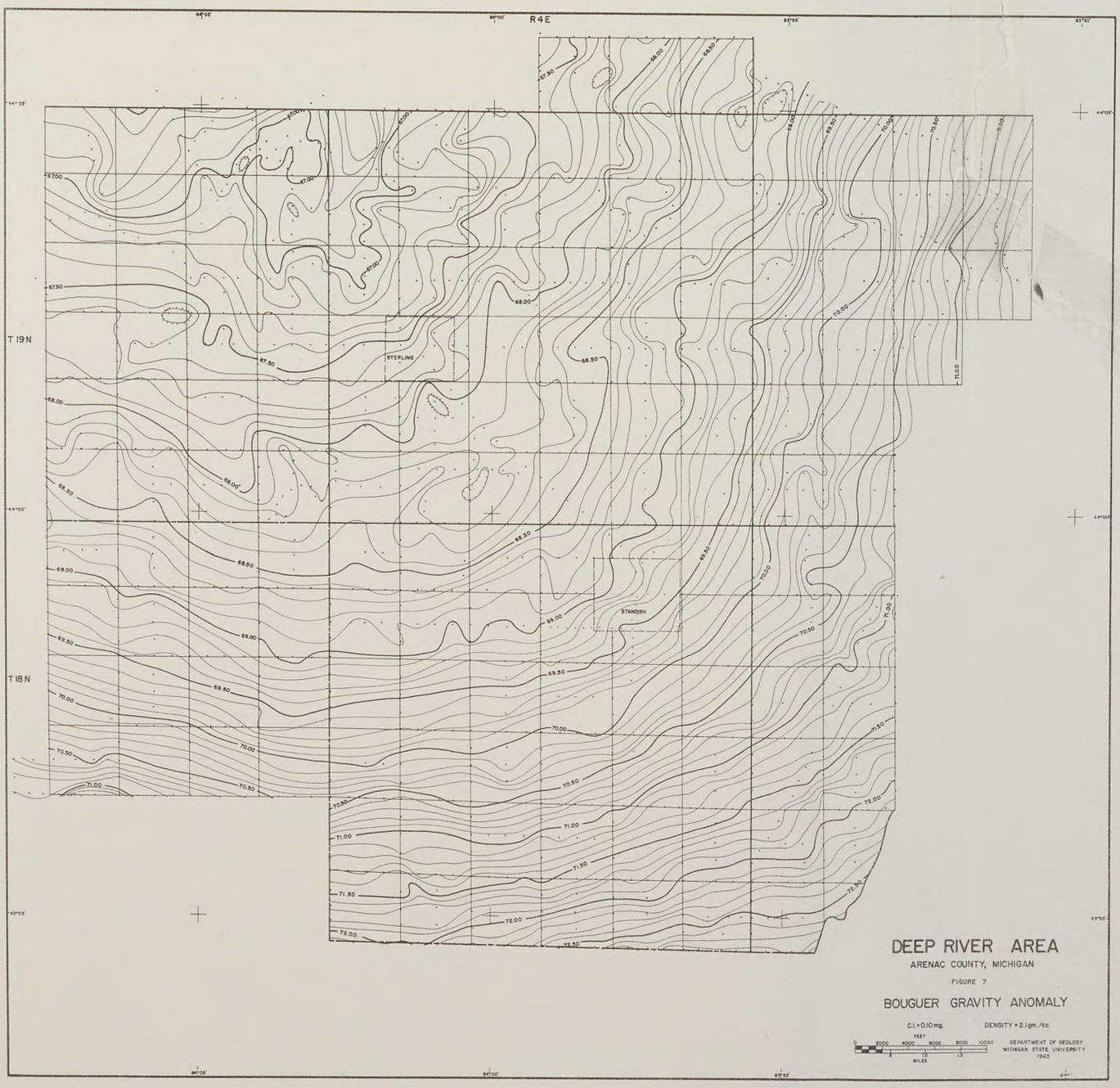

DEEP RIVER AREA

ARENAC COUNTY, MICHIGAN

FIGURE 7

BOUGUER GRAVITY ANOMALY

C.I. = 0.10 mg. DENSITY = 2.1 gm./cc.

FEET 0 2000 4000 6000 8000 10000

MILES 0 .5 1 1.5

DEPARTMENT OF GEOLOGY
MICHIGAN STATE UNIVERSITY
1963

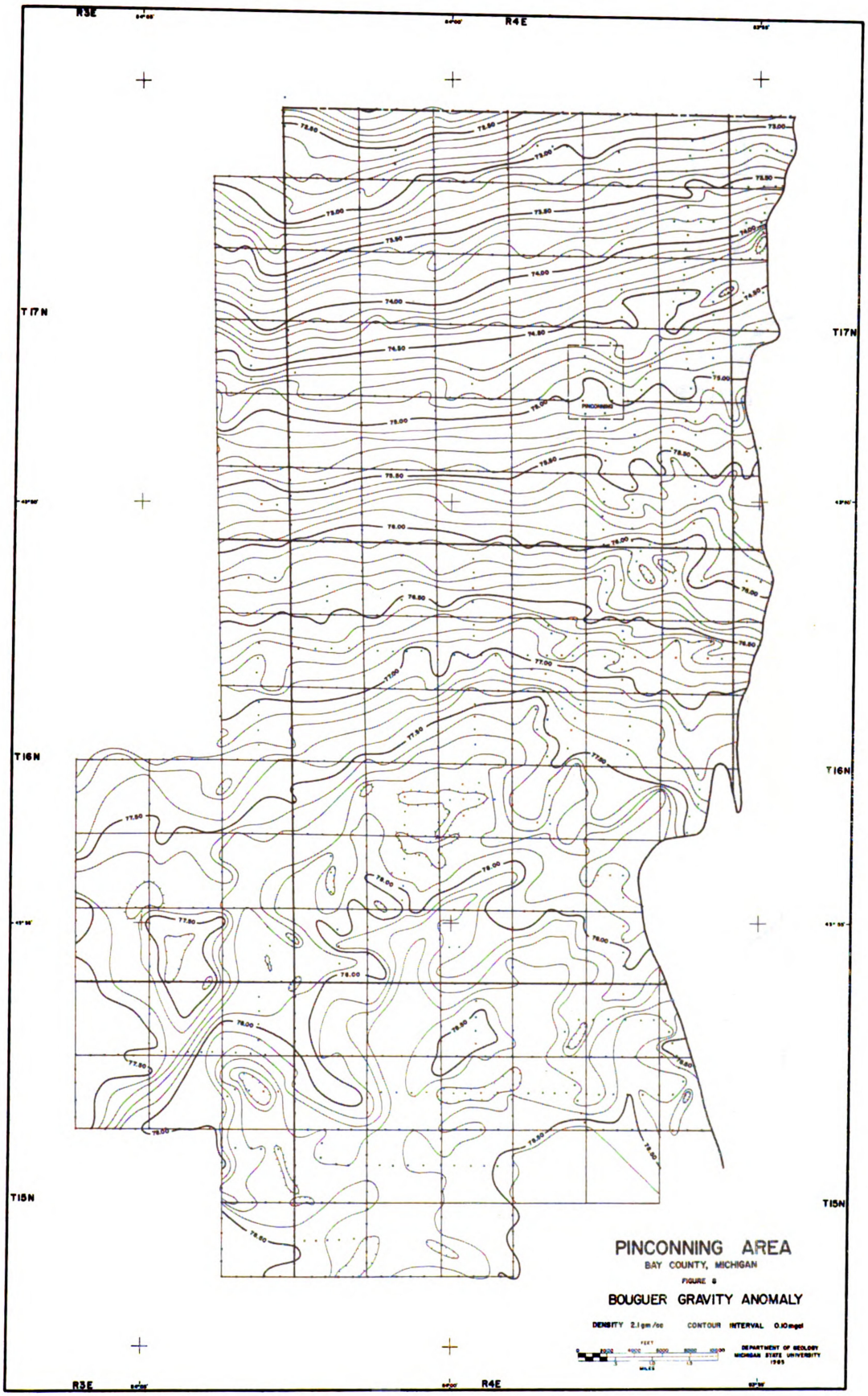
R3E
R4E
T17N
T16N
T15N
PINCONNING
PINCONNING AREA
BAY COUNTY, MICHIGAN
FIGURE 6
BOUGUER GRAVITY ANOMALY
DENSITY 2.1 gm/cc
CONTOUR INTERVAL 0.10 mgal
FEET
MILES
DEPARTMENT OF GEOLOGY
MICHIGAN STATE UNIVERSITY
1965

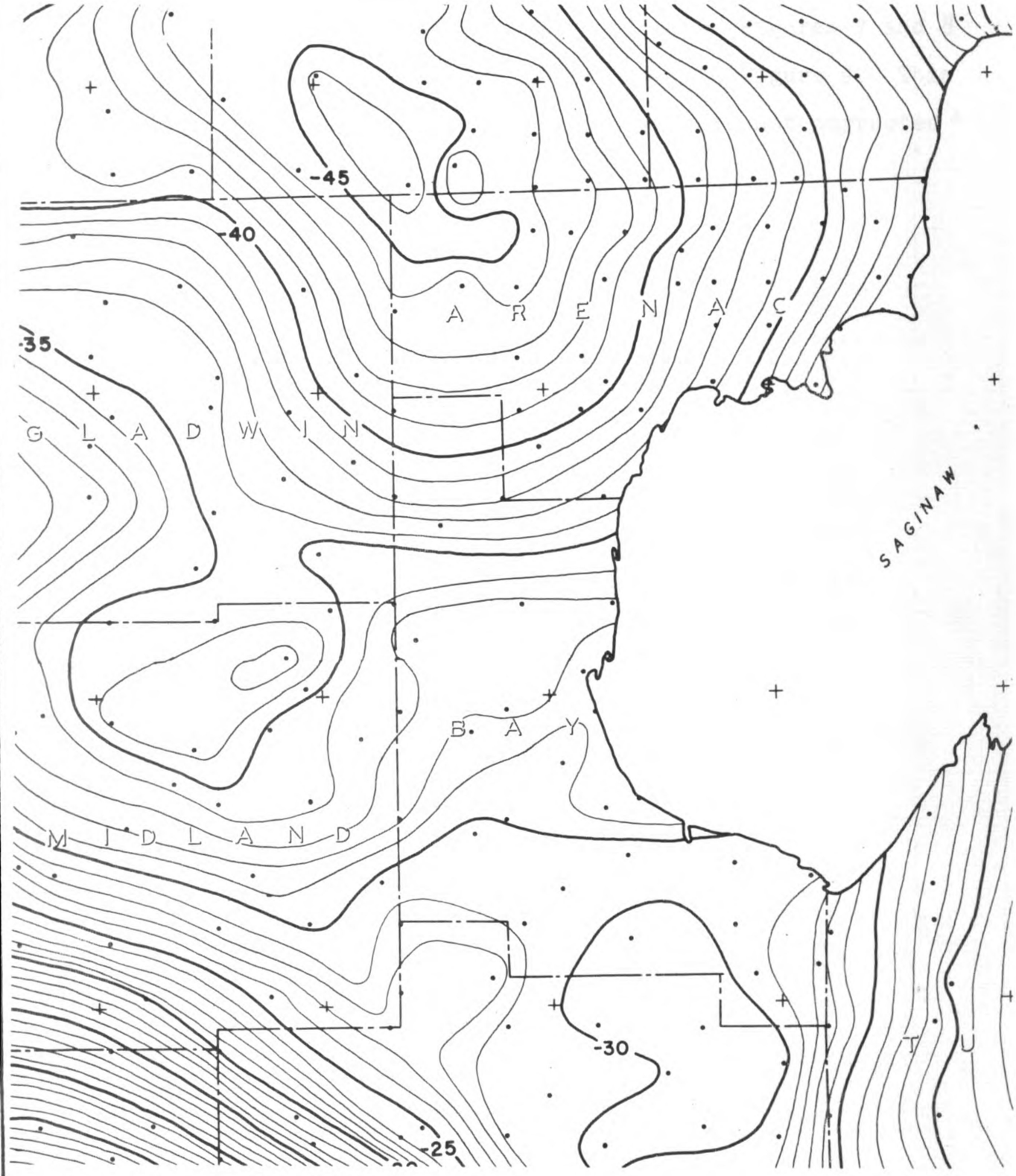

PORTION OF REGIONAL GRAVITY MAP OF MICHIGAN (after HINZE, 1963)

FIGURE 9

The Bouguer gravity anomaly values of Figures 7 and 8 differ from the magnitude of those shown in Figure 9. This is due to the fact that the two surveys were not corrected to the same datum.

CHAPTER VII

INTERPRETATIONAL METHODS

Introduction

The gravity exploration method has been used for a number of years, but the confidence placed in it has been limited. The lack of confidence is due mostly to an inherent problem in gravity interpretation, that of ambiguity of results.

Skeels (1950) has shown that any gravity anomaly produced by one mass can be reproduced by another mass at a shallower depth. Studies in the last decade have helped to defeat this problem by defining the various types of anomalies produced by different features in many geological situations.

Digital computers have been a great help in advancing the status of the gravity exploration method. They now allow many new and older techniques to be used that were once impractical due to the involved mathematics and time consuming arithmetic.

In this study, analytical and statistical methods of interpretation were used much more than graphical methods. Graphical methods were used only to serve as a check of the statistical methods.

Cross-Profiles Graphical Technique

The cross-profile method for the approximation of the regional gravity is a graphical method and is subject to personal bias. This method consists of drawing a smooth curve of the estimated regional gravity gradient along the profile. Sets of profiles are constructed perpendicular to each other. Where one profile crosses another the value of the regional must be the same on each of the perpendicular profiles. Thus, the procedure is to adjust the regional by trial and error until a suitable fit is obtained. The residual gravity values are obtained by subtracting the regional gravity from the value of the Bouguer gravity anomaly at each intersection of the profiles.

This method has the advantage of being a simple way to determine the residual gravity and it permits any knowledge of the area to be used. The method is limited if the residual anomalies are low in magnitude of if the regional gradients are complex.

Three Dimensional Least Squares Statistical Analysis

The least squares method consists of fitting a polynomial equation to a three dimensional surface. In this case the surface consists of X, Y coordinate points and a gravity value at each point giving the third dimension in the Z direction. The polynomial equation is fitted to the surface to a degree where the regional

gravity is adequately defined. In general, the higher the degree of the equation, the better the three dimensional surface is defined. A high degree equation may fit the surface so well that there is no residual anomaly left, while on the other hand, a low degree equation may not adequately define the regional gravity. It is possible that the regional gravity of an area may be so complex that a polynomial equation cannot accurately define it. If this should happen, the least squares method would not be valid.

The principle of the least squares method states that the coefficients of the polynomial equation must be such as to make the sum of the errors a minimum, where the error in this case is the residual gravity or that portion of the surface not fitted by the equation.

The basic polynomial equation used is:

$$\Delta\phi \text{ Regional} = \alpha_{00} + \alpha_{10}X + \alpha_{10}Y + \cdots\cdots + \alpha_{pq}X^{p}\,Y^{q}$$

where

α's = the coefficients of the equation.

The expression can be solved easily by matrices on a digital computer and the resulting gravity value is subtracted from the Bouguer gravity anomaly to give the residual gravity at any point.

Analytical Techniques

Often it is desireable to study the original gravitational field on some plane other than the true plane of observation. The upward continuation method moves the original observation plane farther above the source of the anomalies. Small sharp gradient anomalies that originate near the surface, due to features such as bedrock valleys, may be eliminated while broad lower gradient anomalies due to deeper features are retained. The downward continuation method allows the plane of observation to be brought closer to the source of the anomalies, thus both enhancement and resolution of the anomalies are increased.

Henderson (1960) developed a practical method of approximation for evaluating both the upward and downward continuation equations. This method is outlined in the following paragraphs.

Basically, the problem is to compute the gravity value $\Delta\phi$ (X, Y, Z) above and below the plane of observation. The origin of the right-handed system of coordinates is taken at a point where the field is to be computed, with the Z axis positive vertically downward.

The integral solving the Dirichlet problem for a plane in polar co-ordinates is:

$$\Delta\phi\ (-ma) = \int_0^\infty \frac{ma\Delta\bar{\phi}(r)\ rdr}{(r^2+m^2q^2)^{3/2}}$$

$m = 1, 2, 3, \ldots, n$

(the upward continuation integral)

where (a) is the interval between points, m equals the number of units above the original surface in multiples of (a), and where

$$\Delta\bar{\phi} = \frac{1}{2\pi}\int_0^{2\pi} \Delta\phi\ (r,\theta)\ d\theta \qquad (2)$$

is the average value of $\Delta\phi$ on circles of radius r about the point. Experimentally it was found that radii of r = 0, a, $a\sqrt{2}$, $a\sqrt{5}$, $a\sqrt{8}$, $a\sqrt{13}$, a5, $a\sqrt{50}$, $a\sqrt{136}$, $a\sqrt{275}$, and a25 adequately sample the field. The number of mesh points falling on these radii is respectively 1, 4, 4, 8, 4, 8, 12, 12, 8, 8, and 12. Next a Lagrange interpolation polynomial is fitted to $\Delta\phi$ (0) and the n values $\Delta\phi$ (-ma) computed from (1) to obtain the approximation formula

$$\Delta\phi(z) \simeq \sum_{m=o}^{n} \frac{(-1)^m\ z(z+a)\ (z+2a)\ \cdots\ (z+na)}{a^n\ (z+ma)\ (n-m)!m!}\ \Delta\phi(-ma)\ . \qquad (3)$$

Satisfactory results are obtained from (3) if $n \leq 5$. The mesh interval, a, depends on the data, i.e., the spacing of stations, lateral extent and sharpness of anomalies, etc.

The accuracy of (3) depends on the accuracy of $\Delta\phi(-ma)$ as computed from (1). A numerical integration using a mean value theorem over each integral $r_i \leq r \leq r_{i+1}$ is carried out. The integral (1) is replaced by the sum

$$\Delta\phi(-ma) \approx \sum_{i=o}^{n-1}\left[(r_{i+1} - r_i)^{-1}\int_{r_i}^{r_{i+1}} \Delta\bar{\phi}(r)dr\right] ma$$

$$- \left\{\left[r_i^2 + (ma)^2\right]^{-1/2} - \left[r_{i+1}^2 + (ma)^2\right]^{-1/2}\right\}\left[+O(\frac{1}{r_N})\right] \quad (4)$$

When (a) is set equal to unity, and (4) is evaluated for m = 1, 2, 3, 4, and 5, the five sets of coefficients adopted to upward continuation are obtained. The working formula is expressed as

$$\Delta\phi(-m) \approx \sum_{i=o}^{10} \Delta\bar{\phi}\,(r_i)\; k\,(r_i, m) \quad (5)$$

where $k(r_i, m)$ is the set of coefficients which operate on the center value, and the ten ring average values $\Delta\bar{\phi}(r_i)$ in the computation of $\Delta\phi$ at m grid units above the original plane of observation.

For downward continuation Z is set equal to (a) in equation (3). By successively putting Z = 2a, 3a, 4a, and 5a, formulas are obtained for calculating the gravity on any of the levels below Z = 0, using the same ten ring averages $\Delta\bar{\phi}(r_i)$. The working equation for downward continuation is:

$$\Delta\phi(k) \simeq \sum_{i=0}^{10} \Delta\bar{\phi}(r_i)\, D(r_i, k)$$

where $D(r_i, k)$ is the set of coefficients for computing $\Delta\phi$, k mesh intervals below the original plane of observation.

Second Derivative

The second derivative method is also an important tool in gravity interpretations. This method of analysis tends to emphasize the smaller, shallower geologic features at the expense of larger, deeper features.

Henderson's(1960) method of second derivative analysis was used in this study.

The derivative formulas are obtained from equation (3) by differentiation, when it is placed in the following equivalent form:

$$\Delta\phi\,(z) \simeq -|V|^{-1} \begin{vmatrix} 0 & 1 & -z/a & (z/n)^2 \ldots (-z/a)^n \\ \Delta\phi(0) & 1 & 0 & 0 \ \ldots\ldots\ 0 \\ \Delta\phi(a) & 1 & 1 & 1 \ \ldots\ldots\ 1 \\ \Delta\phi(-2a) & 1 & 2 & 2 \ \ldots\ldots\ 2^n \\ \vdots & & & \\ \Delta\phi(-na) & 1 & n & n^2 \ \ldots\ldots\ n^n \end{vmatrix} \qquad (3a)$$

where $|V|$ is the Vandermode determinant obtained by deleting the first two rows and columns of (3a).

Putting n = 5, equation (3a) is differentiated with respect to z and the first derivative equation is obtained.

$$\frac{\partial(\Delta\phi)}{\partial z} \simeq -(a|V|)^{-1} \begin{vmatrix} 0 & 0 & -1 & 2(z/a) & -3(z/a)^2 & 4(z/a)^3 & -5(z/a)^4 \\ \Delta\phi(0) & 1 & 0 & 0 & 0 & 0 & 0 \\ \Delta\phi(-a) & 1 & 1 & 1 & 1 & 1 & 1 \\ \Delta\phi(-2a) & 1 & 2 & 2^2 & 2^3 & 2^4 & 2^5 \\ \Delta\phi(-3a) & 1 & 3 & 3^2 & 3^3 & 3^4 & 3^5 \\ \Delta\phi(-4a) & 1 & 4 & 4^2 & 4^3 & 4^4 & 4^5 \\ \Delta\phi(-5a) & 1 & 5 & 5^2 & 5^3 & 5^4 & 5^5 \end{vmatrix} . \quad (7)$$

If in (7), z is set equal to zero, the equation for calculating the first vertical derivative on the plane of observation is

$$\left[\frac{\partial(\Delta\phi)}{\partial z}\right]_{z=0} \simeq \frac{1}{a}\left(1 + \frac{1}{2} + \frac{1}{3} + \frac{1}{4} + \frac{1}{5}\right)\Delta\phi(0)$$

$$+ \frac{1}{a} \sum_{m=1}^{5} \frac{(-1)^m\, 5! \cdot \Delta\phi(-ma)}{m^2(m-1)!(5-m)!} \quad .$$

To obtain sets of coefficients for computing $[\partial(\Delta\phi)/\partial z]_{z=k}$ using the ten ring averages $\Delta\overline{\phi}(r_i)$, (a) is set at unity, and (5) is put into (7). The working equation is:

$$\left[\frac{\partial(\Delta\phi)}{\partial z}\right]_{z=k} \simeq \sum_{i=0}^{10} \Delta\overline{\phi}(r_i)\, D'(r_i, k)$$

where $D'(r_i, k)$ are the derivative coefficients appropriate for k mesh intervals below the plane of observation.

The second vertical derivative formula can be obtained by differentiating (7) with respect to z. The resulting working equation is:

$$\left[\frac{\partial^2(\Delta\phi)}{\partial z^2}\right]_{z=k} \approx \sum_{i=0}^{10} \Delta\overline{\phi}\,(r_i)\, D''\,(r_i, k)$$

where $D''\,(r_i, k)$ are the second derivative coefficients appropriate for k mesh intervals below the plane.

Theoretical Gravity Formula

Many geological structures are approximately linear, and the problems connected with them can be solved with two dimensional forms of analysis. The right angle cross section of any two dimensional body can be closely approximated by a polygon, by making the number of sides of this polygon sufficiently large.

The vertical component of gravity due to the polygon can be calculated at any point. This can be done regardless of the size or position of the body. The accuracy depends on how closely the polygon fits the given body. The computations involved in solving for the vertical component of gravity are tedious and lengthy, but are easily programmed for solution by the digital computer. The following mathematical treatment is after Talwani (1959).

The basic mathematical computations are given below. Given an n sided polygon ABCDEF, Figure 10,

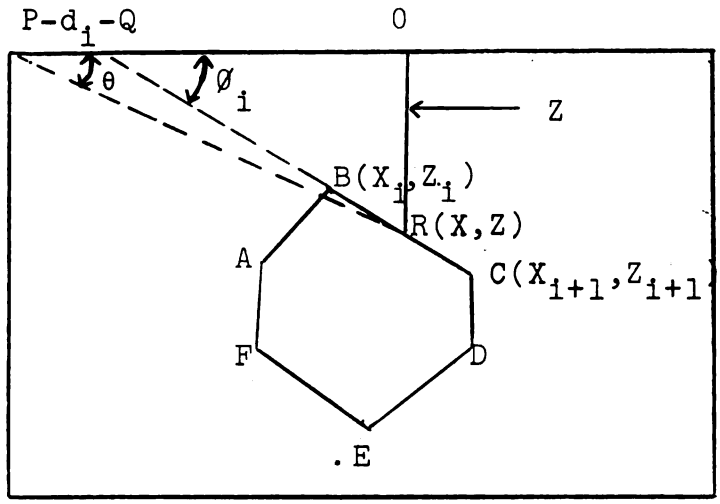

Figure 10

Elements for Talwani's 2D Computations

let P be a point where the gravitational attraction is to be calculated. The point P lies on the XZ plane as does the polygon. Z is defined as positive downwards and θ is measured from the positive X-axis downwards towards the positive Z-axis.

The vertical component of gravity at the origin P has been shown by Hubbert (1948) to equal

$$2G\rho \S z d\theta,$$

where G is the gravitational constant and ρ is the density differential, with the line integral being taken around the periphery of the polygon. The above integral is then evaluated for the given polygon. The contribution of any side of the polygon, for example, side BC, is first computed.

The side BC is projected up to meet the X-axis at Q at an angle of ϕ_i.

Let PQ = a_i, then

$$Z = X \tan \theta \tag{8}$$

for any point R on BC and

$$Z = (X - a_i) \tan \phi_i \tag{9}$$

From (8) and (9)

$$Z = \frac{a_i \tan \theta \tan \phi_i}{\tan \phi - \tan \theta} \tag{10}$$

$$\text{or} \quad \int_{BC} Z \, d\theta = \int_{B}^{C} \frac{a_i \tan \theta \tan \phi_i d\theta}{\tan \phi_i - \tan \theta} \equiv Z_i \tag{11}$$

The vertical component of gravity V is then given as

$$V = 2 G \sum_{i=1}^{n} Z_i \tag{12}$$

with the summations being made over the n sides of the polygon. The above integral must now be solved. In the most general case it can be shown that

$$Z_i = a_i \sin \phi_i \cos \phi_i \left[\theta_i - \theta_{i+1} + \tan \phi_i \log_e \frac{\cos \theta_i (\tan \theta_i - \tan \phi_i)}{\cos \theta_{i+1} (\tan \theta_{i+1} - \tan \phi_i)} \right] \tag{13}$$

where

$$\theta_i = \tan^{-1} \frac{Z_i}{X_i} \tag{14}$$

$$\phi_i = \tan^{-1} \frac{Z_{i+1} - Z_i}{X_{i+1} - X_i} \tag{15}$$

and

$$\theta_{i+1} = \tan^{-1} \frac{Z_{i+1}}{X_{i+1}} \tag{16}$$

$$a_i = X_{i+1} + Z_{i+1} \frac{X_{i+1} - X_i}{Z_i - Z_{i+1}} \tag{17}$$

It should be noted that θ_i, θ_{i+1}, $\emptyset_i$, and a_i can all be explicitly expressed in terms of the X_i's and Z_i's. This is especially advantageous, since one of the simplest ways of defining the boundaries of a body is to specify the coordinates of adjacent points at the vertices of the body.

CHAPTER VIII

INTERPRETATION

Gravity Effects of Bedrock Valleys

The gravity effects of near surface features must first be determined to isolate gravity anomalies originating from deeper geological features of immediate interest to this study. The three dimensional least squares method was used to determine these effects. The residual gravity maps obtained from this method are shown in Figures 11 and 12. They are residuals from the fifth degree least squares fit. The third and seventh degree fits also were studied, but are not shown because they showed essentially the same picture. The third degree fit showed the anomalies to be slightly broader, and the seventh degree fit showed them to be slightly narrower.

Several gravity minima can be seen on Figures 11 and 12. It is doubtful that all the negative anomalies are due to bedrock valleys, but the narrow linear gravity minima seemingly would be due to the valleys. In the study area where there is good subsurface control, bedrock valleys have been outlined and have negative anomalies associated with them.

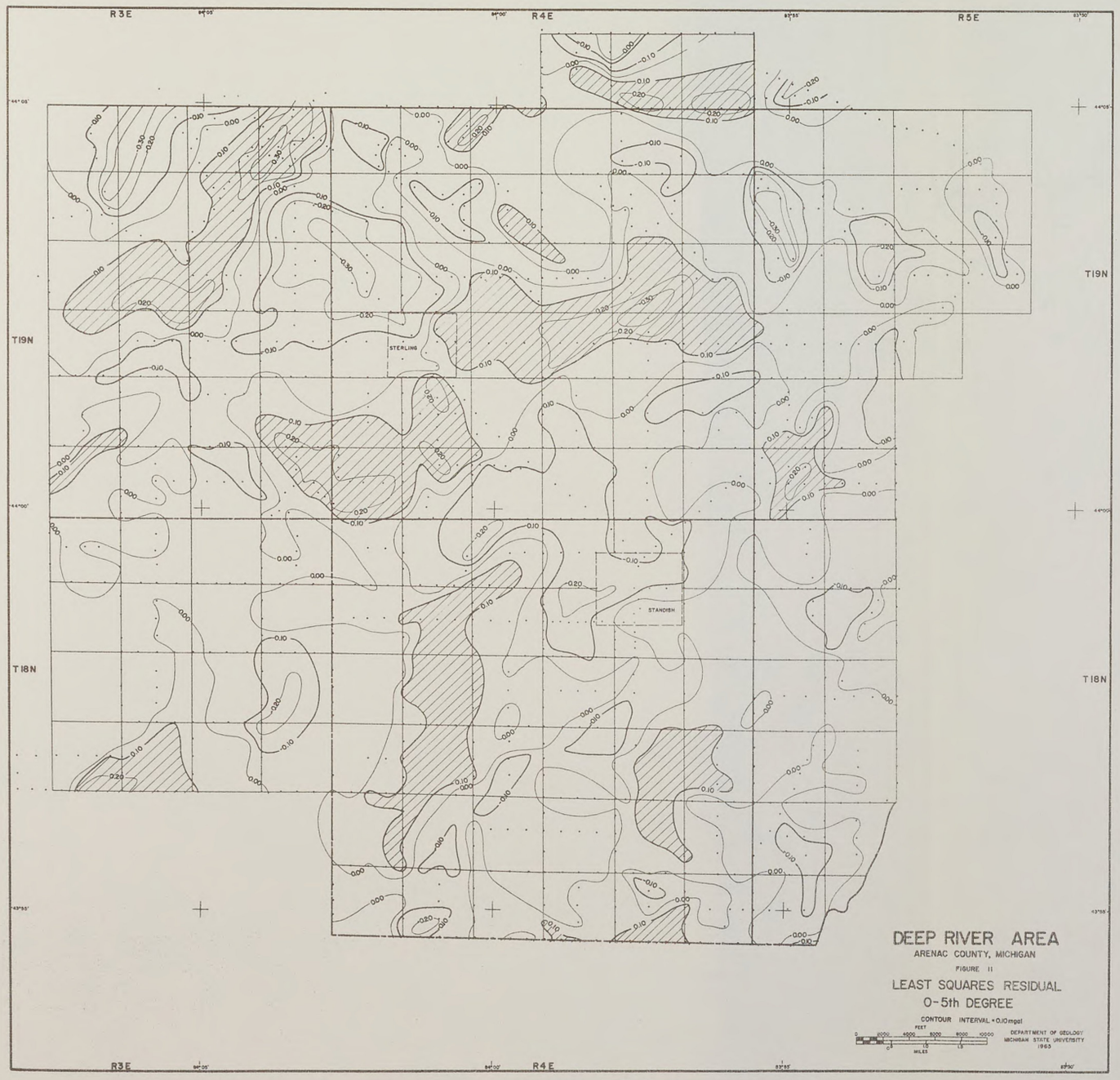
R3E
R4E
R5E
T19N
T18N
STERLING
STANDISH
DEEP RIVER AREA
ARENAC COUNTY, MICHIGAN
FIGURE 11
LEAST SQUARES RESIDUAL
0-5th DEGREE
CONTOUR INTERVAL = 0.10 mgal
FEET
MILES
DEPARTMENT OF GEOLOGY
MICHIGAN STATE UNIVERSITY
1965

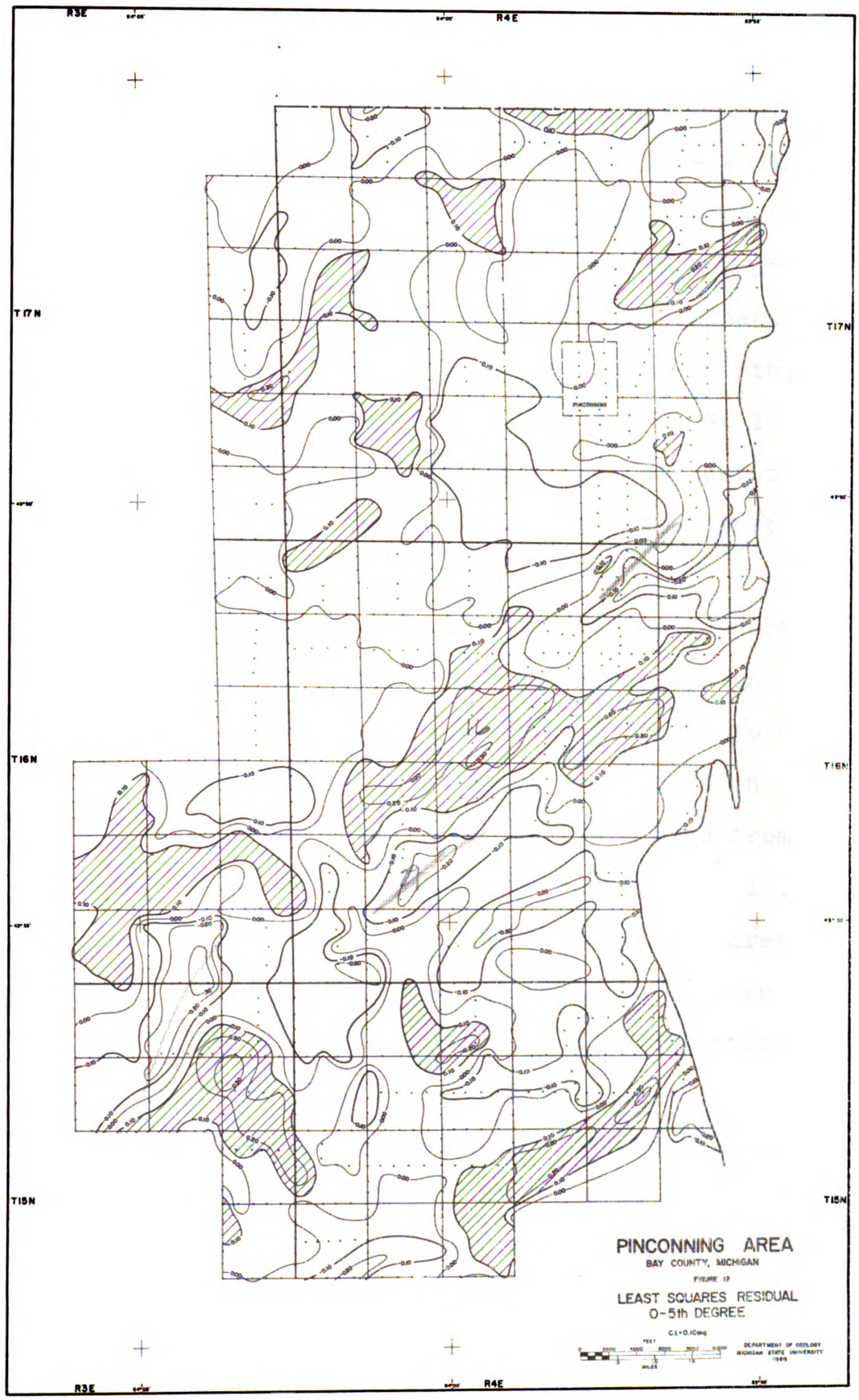
R3E
R4E
T17N
T16N
T15N
PINCONNING
PINCONNING AREA
BAY COUNTY, MICHIGAN
FIGURE 17
LEAST SQUARES RESIDUAL
0-5th DEGREE
C.I.=0.1C/cm
FEET
MILES
DEPARTMENT OF GEOLOGY
MICHIGAN STATE UNIVERSITY
1969

Figure 13 is a map of the bedrock topography for the Deep River area. Three channels are well outlined in this area. One is coincident with the northwestern end of the Deep River fracture zone. It can be traced in a southeast direction from section 1, thru 8, 9, 15, 16, and partially into section 21. At this point it turns south and joins a large bedrock low in section 22, extending southeast through sections 28, 34, and 35, of Township 19 north, Range 4 east. It continues on into sections 2, 3, 10, and 11 of Township 18 north, Range 4 east. At this point it appears to end. It may, however, turn in a southwest direction and continue off the map.

A second channel can be seen in Township 10 north, Range 3 east. It trends in a northeast direction and runs entirely across the township. It appears to join the above mentioned valley in the region of section 6 in Township 19 North, Range 4 east. It can be traced from there in a southeast direction through sections 1, 12, 13, 14, 23, 27, and 28 where it runs out of the study area.

Another channel, less well defined, can be seen in the extreme northwest portion of Figure 13. It covers most of section 4 and part of section 9. There is only one well shown that controls this channel, but its trend was inferred from other well logs studied that were outside of the study area and are not shown on the figure.

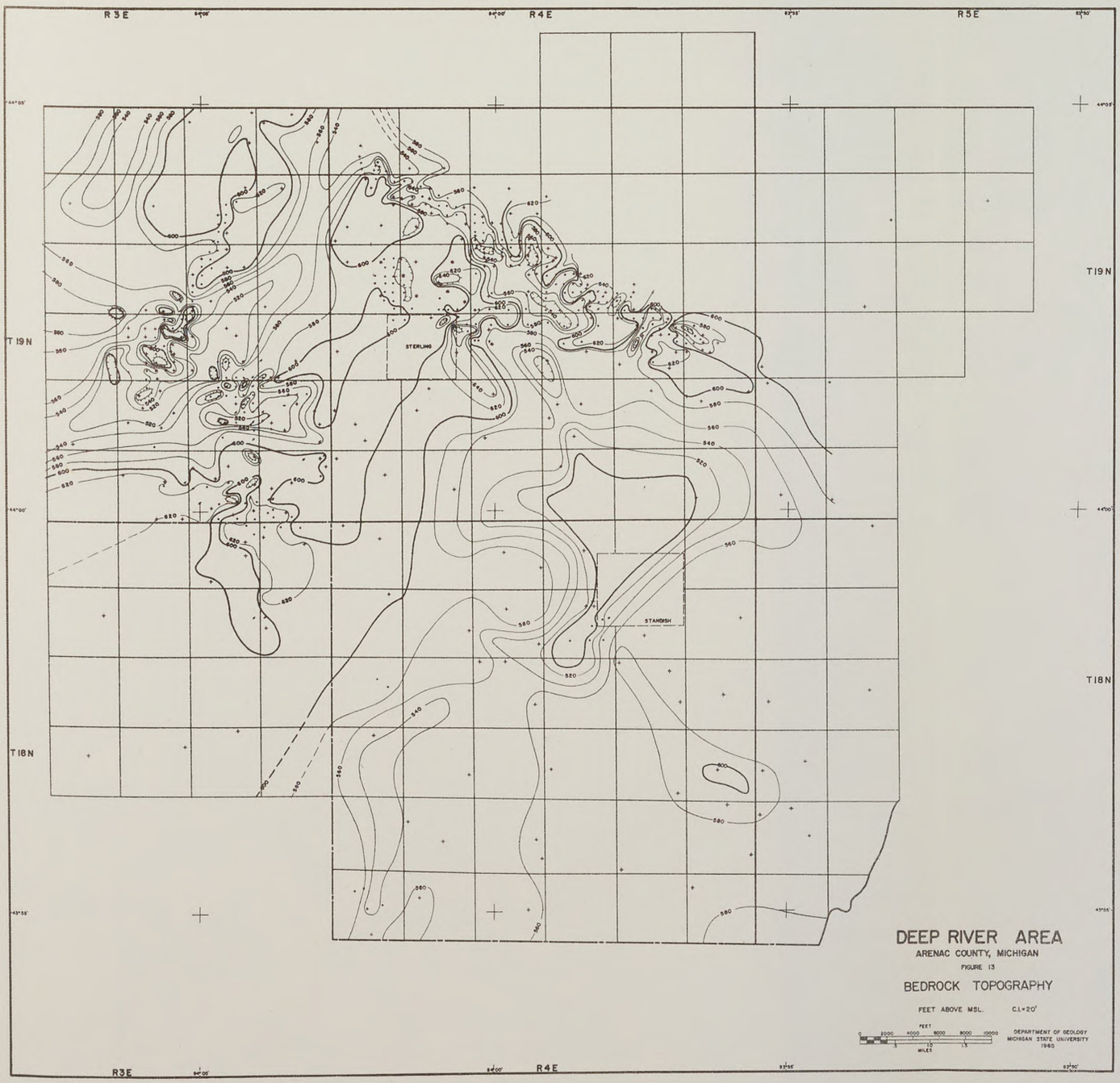

DEEP RIVER AREA

ARENAC COUNTY, MICHIGAN

FIGURE 13

BEDROCK TOPOGRAPHY

FEET ABOVE MSL. C.I.=20'

DEPARTMENT OF GEOLOGY
MICHIGAN STATE UNIVERSITY
1963

By comparing Figures 12 and 13, the relation between the bedrock valleys and negative gravity anomalies can be seen. Only in the case of the last valley mentioned is there a good correlation. In the other cases the negative anomalies do not follow the entire length of a channel, but rather appear as small isolated anomalies along the trend of the valley. Possible explanations for this will be discussed later.

Figure 14 is a map of the bedrock topography in the Pinconning area. Due to the extreme lack of subsurface control over most of this area, the isolation of bedrock valleys is difficult. Only one channel can be seen. It is located in the northeastern portion of Township 16 north, Range 4 east, where it appears to begin. It broadens and trends south through sections 2, 11, 12, 13, and 14, where it starts to turn to the west. In the area where it is trending in a westerly direction, it is much too shallow to be capable of producing an anomaly of much more than -.02 mgals. This is much too small to be detected.

By comparing Figure 12, the residual gravity of the area, to Figure 14, the bedrock topography, it can be seen that there are a number of narrow linear negative anomalies in the area where the above mentioned valley is very broad. Several of these follow the axis of the broad trough.

This area of negative anomalies can be followed across the map in a northeast-southwest direction. The negative

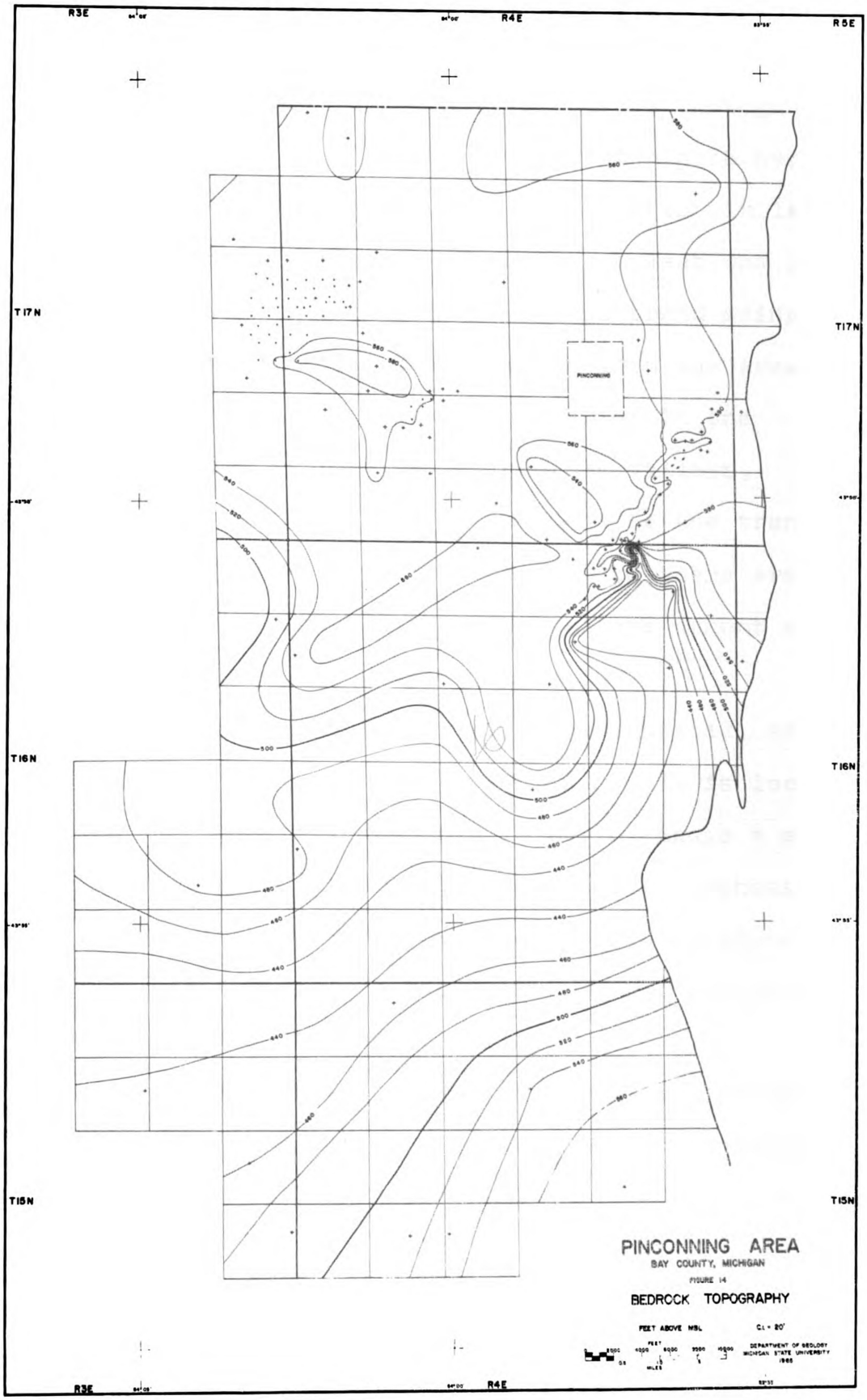
R3E
R4E
R5E
T17N
T16N
T15N
PINCONNING
PINCONNING AREA
BAY COUNTY, MICHIGAN
FIGURE 14
BEDROCK TOPOGRAPHY
FEET ABOVE MSL
C.I. = 20'
DEPARTMENT OF GEOLOGY
MICHIGAN STATE UNIVERSITY
1966

trend runs through sections 1, 2, and 10 of Township 15 north, Range 3 east, into sections 35 and 36 of Township 16 north, Range 3 east. From there it passes through sections 30, 29, 28, 27, 21, and 20 of Township 16 north, Range 4 east. Here it is paralleled by another similar sized negative anomaly just to the south in sections 33, 35, 27, 26, and 25. From section 25, this trend swings north as does the one recognizable channel in the area.

The above mentioned negative anomalies in the Pinconning area may well be due to bedrock valleys, especially since their trend is coincident to the trend of the large bedrock valley. However, since there are practically no wells in the area, the valleys cannot be traced on the bedrock topography map.

In the extreme southern portion of Figure 12, another narrow linear negative anomaly can be seen. It is located in sections 19 and 20 of Township 15 north, Range 4 east. Another negative anomaly about 2 miles to the northeast also is shown. Perhaps these two anomalies also represent a bedrock valley trending to the northeast and possibly merging with the other proposed valley.

Figure 15 is a cross section of a typical bedrock channel for the area. Both the observed and theoretical anomalies are shown. The theoretical and observed anomalies have approximately the same magnitude, but the centers of the anomalies are not coincident. This is due to the

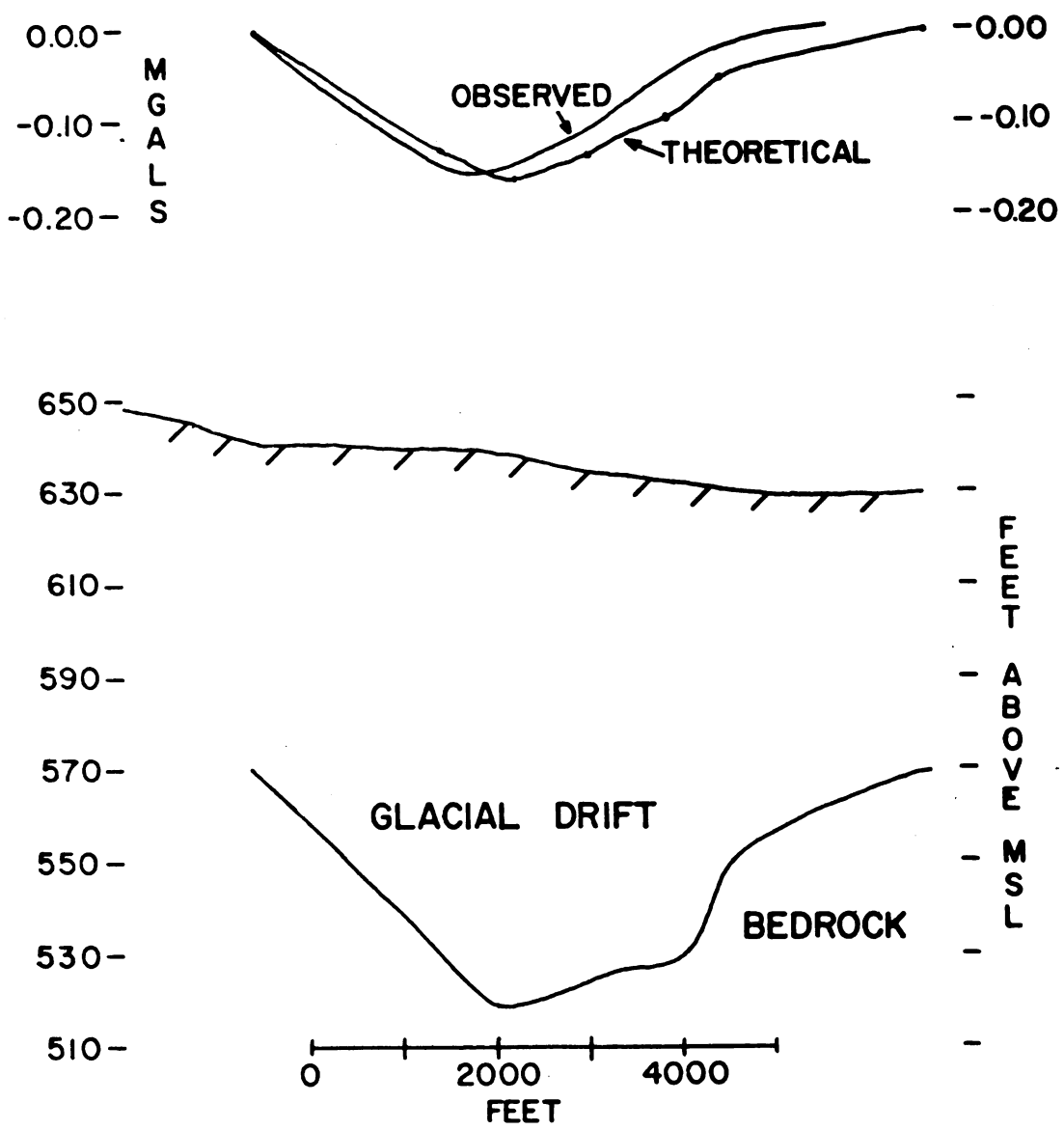

TYPICAL BEDROCK VALLEY WITH OBSERVED AND THEORETICAL ANOMALIES

FIGURE 15

assumed polygon used in Talwani's two dimensional computation, for calculating the theoretical anomaly. The sides of the polygon correspond to the outline of the channel which was taken from the bedrock topography map. By slightly adjusting the size and the position of the valley, the theoretical anomaly can be made to correspond closely with the observed anomaly. The magnetude of the anomaly can be changed by changing the density differential. In this case a density differential of -0.2 gm/cc was used in calculating the theoretical anomaly.

As previously stated, the gravity minima do not delineate the valleys as well as might be expected. In most cases there are a number of isolated lows associated with the valleys. This may be due to effects from deeper features. For example, a deeper body that has a positive anomaly associated with it, may superimpose itself easily on the negative anomaly due to the valley. Positive and negative anomalies of similar magnitude may cancel each other out. In this case a truly anomalous area may show up as no anomaly.

Possible variations in the density of the glacial drift in the channels could distort the anomaly due to the valley. Also, slight changes in the density of the material in the sedimentary column may distort the anomalies.

From this portion of the study, it was concluded that bedrock channels in the study area can produce negative anomalies of magnitude large enough to mask anomalies due to deeper features. When the bedrock topography is known the gravity effects of the valleys can be calculated using Talwani's two dimensional method, and they can be removed from the Bouguer gravity. One way of removing these effects is by the cross-profile method. The effects also may be removed by the upward continuation method.

Gravity Effects of Fracture Zones

Effects on the Bouguer gravity of the several known fracture zones of the study area must be determined before the zones can be isolated. There are several variables that must be considered in calculating the effects of the fracture zones.

The density differential between the porous dolomite of the fracture zone and the surrounding tight limestone first must be determined. From density measurements made on several well samples from the area, it was determined that the limestone has a density of 2.701 gm/cc. A value of 2.85 gm/cc was determined for the dolomite taken from the producing zone. If the samples of dolomite are truly representative of the fracture zone, a positive density differential of 0.149 gm/cc would be produced. However, when the porosity of the fracture is considered, the density differential may vary considerably.

Figure 16, modified after Goldich and Parmelee (1947), is a graph of the density and porosity relationships of dolomite and limestone assuming that all pore space is water saturated. The values used to produce this graph were determined from measurements made on 75 samples from the Ellenburger group of Texas. It was found that the average density of limestone is 2.705 gm/cc and its average porosity is 0.5 per cent. The properties of dolomite were found to be more variable than those of limestone. The average grain density of dolomite varied from 2.811 to 2.848; its porosity ranged from 1.1 to 12.6 per cent. The calculated calcite content ranged from 2.7 to 27.2 per cent and the calculated dolomite content ranged from 70 to 94.7 per cent.

With the above ranges of possible chemical and physical properties of limestone and dolomite in mind, the effects of the fracture zones on the Bouguer gravity anomaly must now be considered. From Figure 16, the possible expected density differential can be determined. For example, a rock of 100 per cent dolomite content with porosity of 5 per cent would have a density of 2.755 gm/cc. A limestone with 1 per cent porosity would have a density of 2.688 gm/cc. Thus, a positive density differential of 0.067 gm/cc is produced.

Figure 16 shows that either a positive or a negative density differential is possible. A pure dolomite with 10 per cent porosity, surrounded by a pure limestone of 1 per

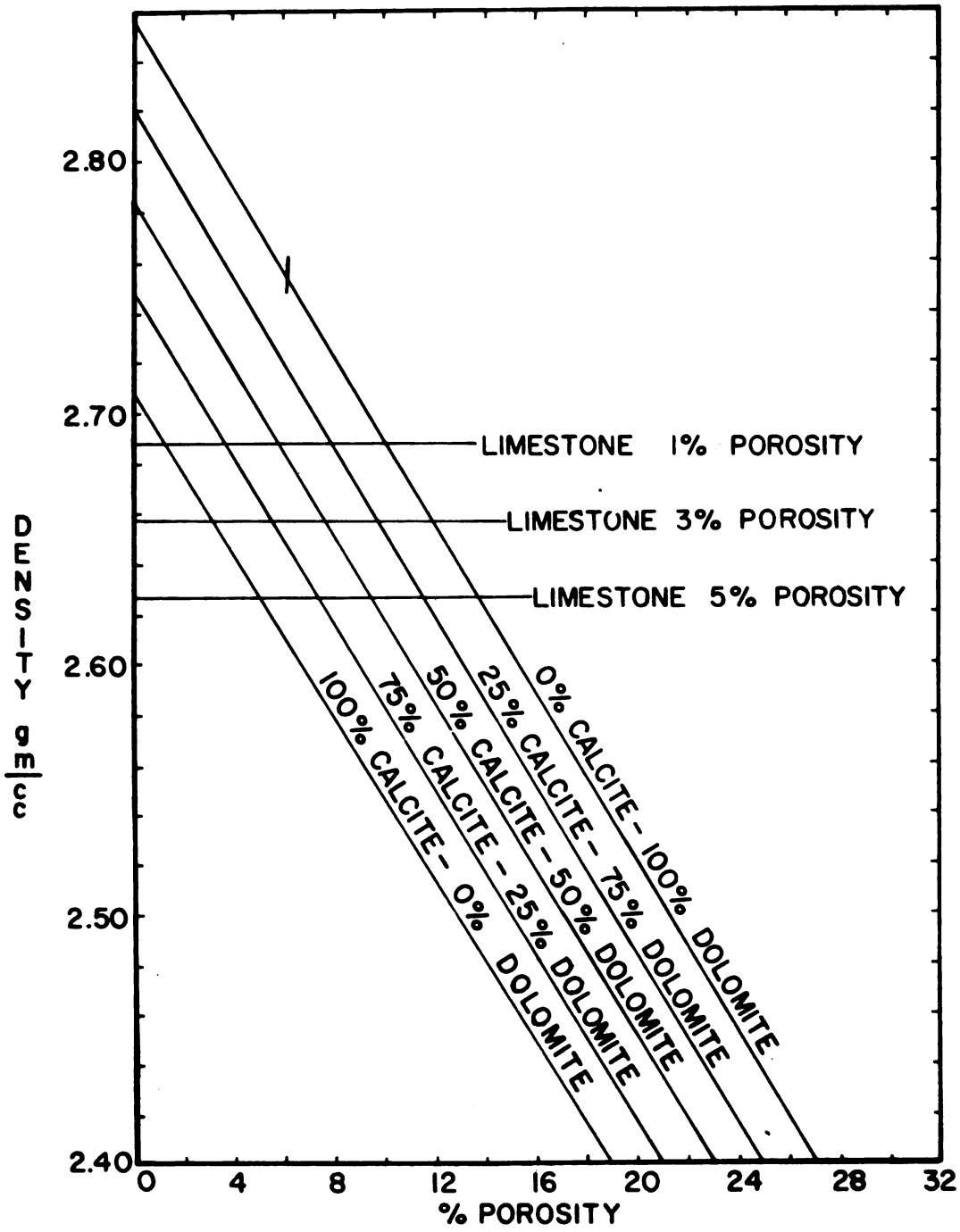

DENSITY AND POROSITY RELATIONSHIPS OF WATER SATURATED DOLOMITE AND LIMESTONE

FIGURE 16

cent porosity would produce no density differential. In this case, it would be impossible to detect the fracture zones by the gravity method.

It is felt that the dolomite of the fracture zones is fairly pure due to its secondary nature of deposition. It is assumed that the limestone is fairly pure. Assuming that the limestone has less than 1 per cent porosity, a positive density differential would occur as long as the porosity of the dolomite does not exceed 10 per cent.

It is also felt that the porosity of the fracture zones may be extremely irregular. This is suggested by the fact that some of the wells in the Deep River and North Adams Fields are prolific producers, and in some cases, adjacent wells exhibit poor production. The high production of some of the wells also suggests that the porosity of the zones may exceed 10 per cent in some instances. These two possible variations would produce various anomalies over the fracture zones.

The depth to the top of the fracture zones, as well as their width and depth must also be considered. From Figures 5 and 6, it can be seen that the top of the producing zone in the Deep River Field is about 2050 feet below mean sea level, and the North Adams producing zone is about 2100 feet below mean sea level. The top of the producing zone in the Pinconning Field is slightly over 2200 feet below sea level. The approximate average

elevation of the area is 600 feet. This would place the depth to the top of these features at approximately 2800 feet. This figure was held constant when computing the theoretical anomalies of various width fracture zones.

The depth to the bottom of the fracture zones cannot exceed 3700 feet. Two dimensional computations indicate that the theoretical anomaly produced by a body with a bottom depth of much more than 3700 feet is much larger than any observed anomaly of the area.

Figures 17 and 18 show the theoretical anomaly over fracture zones of varying width. Positive density differentials of 0.075, 0.100, 0.125, and 0.150 gm/cc were used in the calculations. A bottom depth of 3400 feet was utilized. This would place the bottom depth of the fracture zone in the Lucas formation. It is assumed that the entire Rogers City-Dundee interval is fractured.

Figures 17 and 18 show that many various magnitude anomalies can be produced under varying conditions. For example, a fracture zone 2000 feet wide might produce an anomaly varying from 0.13 to 0.27 mgals, depending on the density differential between the fracture zone and the surrounding limestone.

The smallest magnitude anomaly shown in the figures is 0.06 mgals. It would be extremely difficult to detect a fracture zone producing an anomaly of only 0.10 mgals or less.

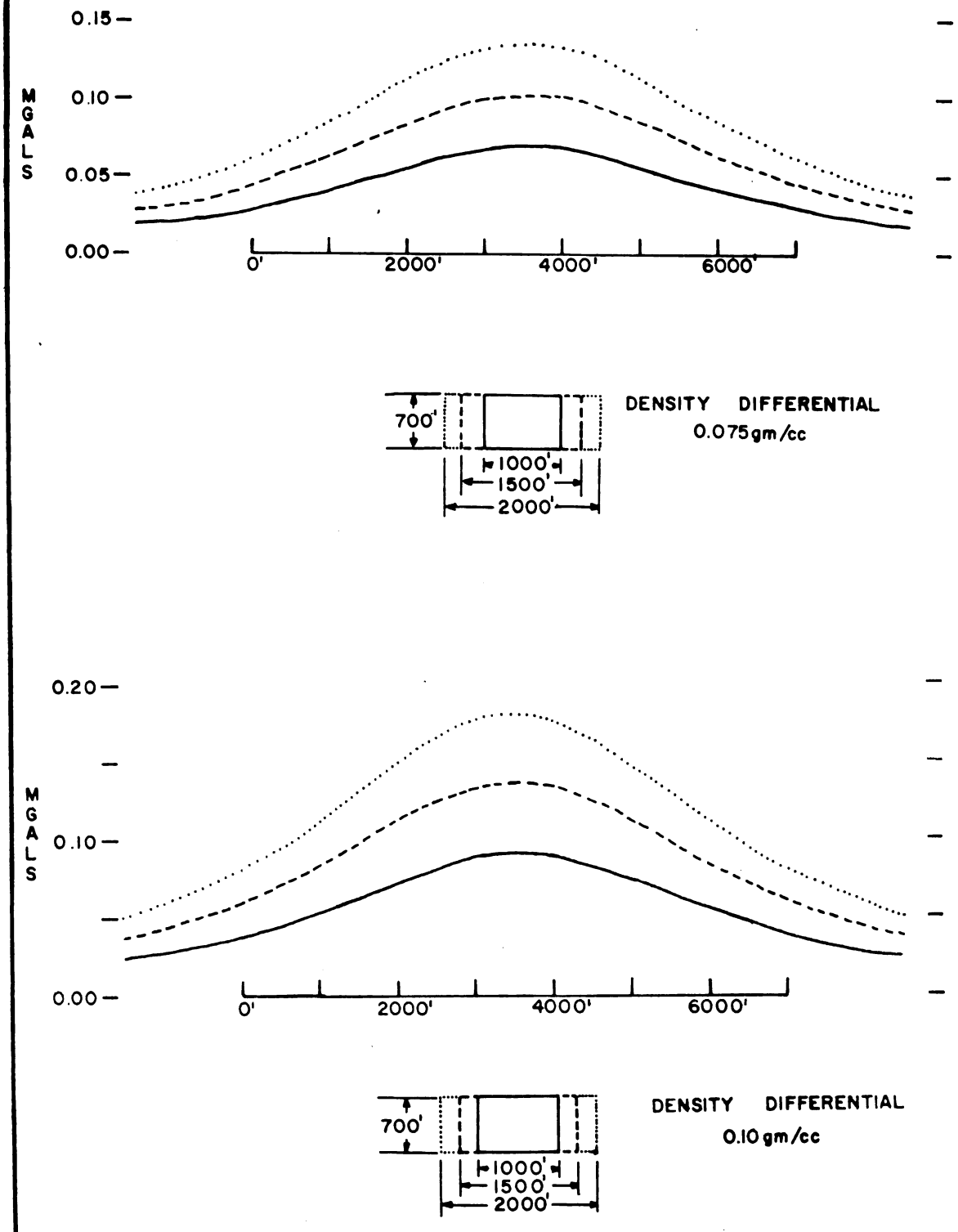

THEORETICAL ANOMALIES FOR VARIOUS WIDTH FRACTURE ZONES 2800 FEET BELOW THE SURFACE

FIGURE 17

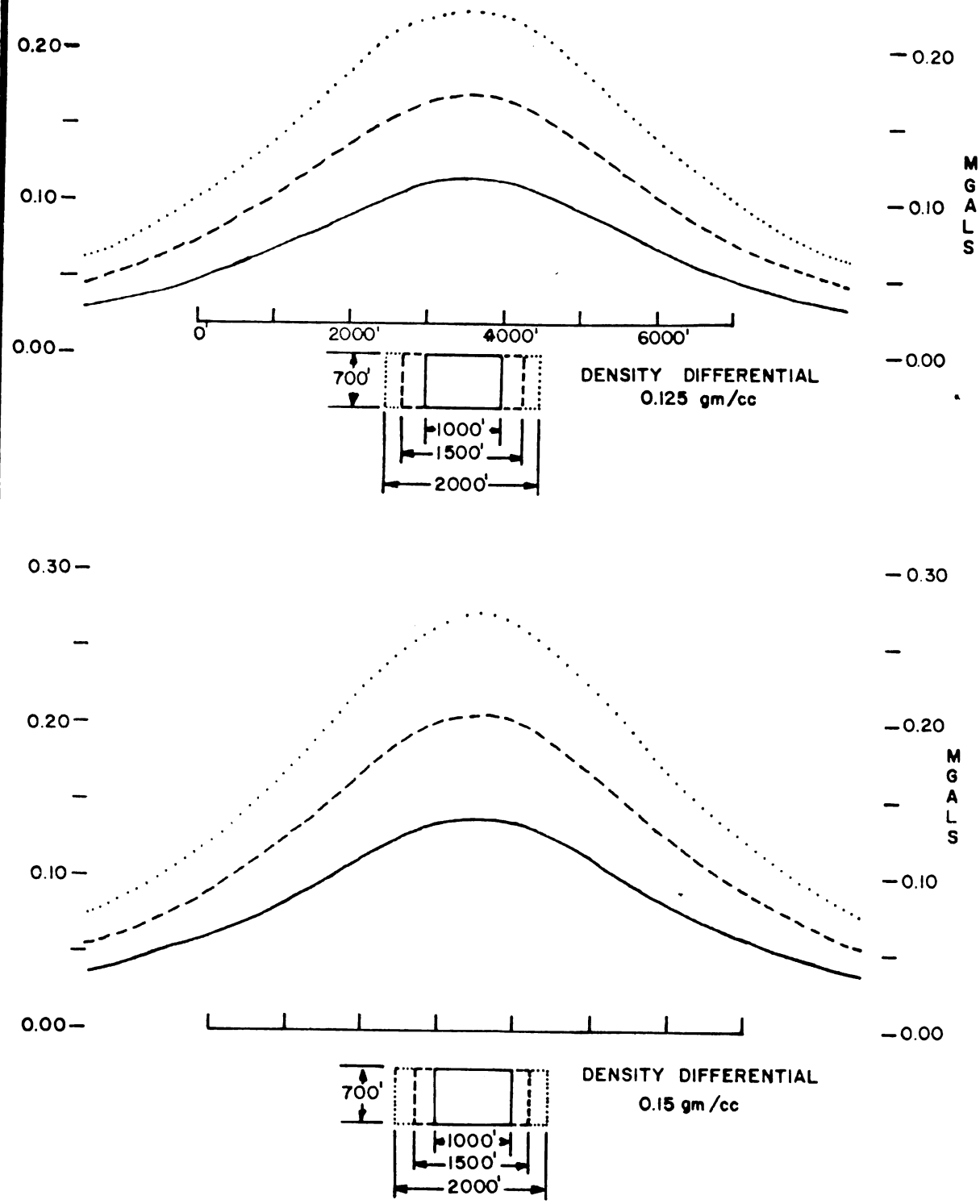

THEORETICAL ANOMALIES FOR VARIOUS WIDTH FRACTURE ZONES 2800 FEET BELOW THE SURFACE

FIGURE 18

The largest anomaly seen on Figures 17 and 18 is 0.27 mgals. It must be realized here that the range of anomalies shown, 0.06 to 0.27 mgals, certainly is not the entire range in magnitude of anomalies that might be produced by various fracture zones. However, it is felt that this range is applicable for the fracture zones in this study area.

In summary, it was concluded from this part of the study, that the fracture zones of the study area may or may not produce anomalies of detectable magnitude. Due to the many variables involved, anomalies of widely varying characteristics might be produced. It is more likely that the fracture zones would produce positive anomalies, rather than negative anomalies, if an anomaly is produced. If the amplitude of the anomalies is less than 0.10 mgals, they would be extremely difficult to detect.

Gravity Effects of Regional Structures

From Figures 5 and 6 it can be seen that there are several regional structures in the area. The Deep River anticline and the large syncline in the eastern portion of the Pinconning area outlined by dashed contour lines are the most important features here. There is also another anticline indicated in the extreme southern portion of the Pinconning area. These features show no relation, either positive or negative, to the gravity picture. It is expected that these features would produce detectable

anomalies. It is felt that there is no correlation between these features and the gravity picture because there is no appreciable density difference between the features and their surroundings.

Bouguer Gravity Anomaly Map

The Bouguer gravity anomaly map indicates a gravity maximum coincident with the North Adams Field. This may be fortuitous, but this is unlikely because the strike of the anomaly is parallel with the North Adams Field. The magnitude of the anomaly is about 0.15 mgals and would be about 3000 feet wide when separated from the regional gravity. The magnitude of the anomaly is reasonable when compared with theoretical calculations made previously.

There is no indication of the Deep River or North Adams fracture zones on the Bouguer gravity anomaly map. There is a bedrock valley coincident with the northern end of the Deep River fracture zone. However, if the zone was producing an anomaly it should be present at least over the southern end of the field where it would not be masked by the negative anomaly due to the valley.

The Pinconning fracture zone also has no anomaly associated with it. This was more or less expected, due to the width of this fracture zone. From the theoretical studies it can be seen that a fracture zone of this size would product an anomaly of 0.10 mgals or less, in which

case it would be extremely difficult to detect by the gravity exploration method.

It also can be seen from the Bouguer gravity anomaly map, that there are two areas of gentle regional gravity gradients. These areas are in the northern portion of the study area in the vicinity of the North Adams and Deep River Fields and in the extreme southern portion of the study area. The regional gravity gradient between these two areas is much steeper. The gravity in the two areas of gentle regional gradient appears more complex than in the remaining area simply because of the gentle regional gradients.

Other possible sources of this complexity were studied. It is possible that lateral variations in the density of near surface materials, both the glacial drift and the bedrock, could cause such an effect. However, there is no indication of lateral density variations of this material in the area.

Least Squares Residual Anomaly Map

The least squares residual anomaly map of the study area indicates the presence of the North Adams fracture zone. There is a positive anomaly of greater than 0.10 mgals coincident with the northern three-quarters of the zone. The anomaly is centered over the fracture zone and is parallel in strike. It averages about 3000 feet in width where it is coincident with the fracture zone.

From theoretical studies of the effects on gravity due to fracture zones, it was concluded that an anomaly of this size and magnitude is approximately what is expected for a fracture zone of this size.

The anomaly is not coincident with the North Adams fracture at its southern limit, but rather is shifted one-half mile to the west. In the area where the anomaly and the fracture zone are no longer coincident, both the structure and bedrock topography become irregular. It is possible that both of these changes have a distorting effect on the anomaly. The least squares residual map shows no indication of the Deep River or Pinconning fracture zones. This was expected since there was no indication of them on the Bouguer gravity anomaly map. As previously stated, there is a bedrock valley coincident with the northern end of the Deep River Field, and it is detected on the least squares residual map. It is not outlined as well as expected, but reasons for this were discussed previously. Again, if the Deep River fracture zone was producing an anomaly, some indication of it should be shown at least over the portion of the fracture zone not effected by the bedrock valley.

There are two other anomalies shown on the least squares maps that may be indicative of fracture zones. They are both roughly parallel to the strike of the North Adams fracture. The first of these anomalies is located in

Township 18 north, Range 4 east. It covers most of sections 8, 17, and 20 and runs partially into section 4 at its northern extent. It covers parts of sections 29 and 30 in its southern extremity. It is felt that since this anomaly is parallel to the North Adams anomaly, that it may possibly be due to a fracture zone of similar nature. However, this anomaly does not reach a magnitude of 0.20 mgals as the North Adams anomaly does.

The other anomaly can be seen in the extreme southern portion of the Pinconning area. This anomaly corresponds less well to the strike of the North Adams anomaly. It is felt that this anomaly is not delineated well because it is close to the edge of the study area and the least squares method may not define accurately the regional anomaly in this area.

From this portion of the study it was concluded that the North Adams fracture zone is producing a positive anomaly and it has been detected. It is felt that since the North Adams fracture zone is less well developed than the Deep River fracture zone, its overall porosity is less and a larger positive density differential is therefore created resulting in a detectable gravity anomaly.

The Deep River fracture probably is not producing an anomaly of sufficient magnitude to be detected. It is felt that this is due to the increased porosity of this zone over that of the North Adams fracture zone. Since this

fracture zone is longer and broader than the North Adams fracture, it certainly should produce a detectable anomaly if the overall porosity of the fracture was the same as the North Adams fracture zone.

The Pinconning fracture is much smaller than the other two known fractures and therefore has no detectable anomaly associated with it. This is substantiated by theoretical calculations.

Upward, Downward and Second Vertical Derivative Methods

Profiles of upward continued, downward continued, and second vertical derivative values over the North Adams and Deep River Fields are shown in Figures 19 and 20. The methods used in determining these profiles are discussed previously in the section on interpretational methods. All of these methods employed a mesh interval of 1000 feet. The original Bouguer surface was upward continued 3000 feet and downward continued 2000 feet. Second derivatives were calculated on the original Bouguer surface.

The upward continuation method eliminates most of the small sharp gradient anomalies due to near surface features and retains the broad anomalies due to deeper sources. The downward continuation and second vertical derivative methods applied to the original Bouguer surface accentuates the small sharp gradient anomalies somewhat at the expense of broader anomalies due to deeper features.

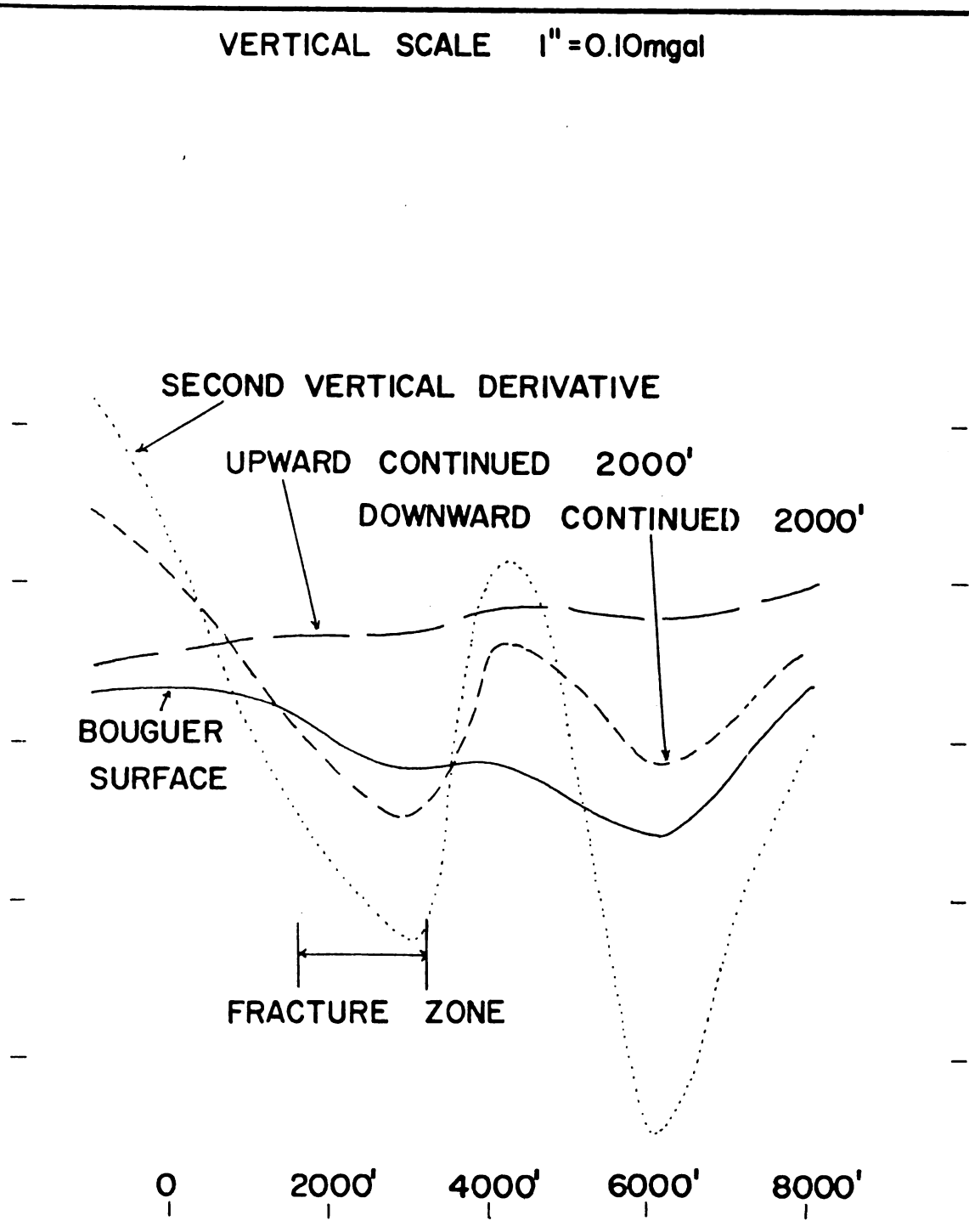

PROFILES OF ANALYTICAL METHODS OVER THE DEEP RIVER FRACTURE ZONE

FIGURE 19

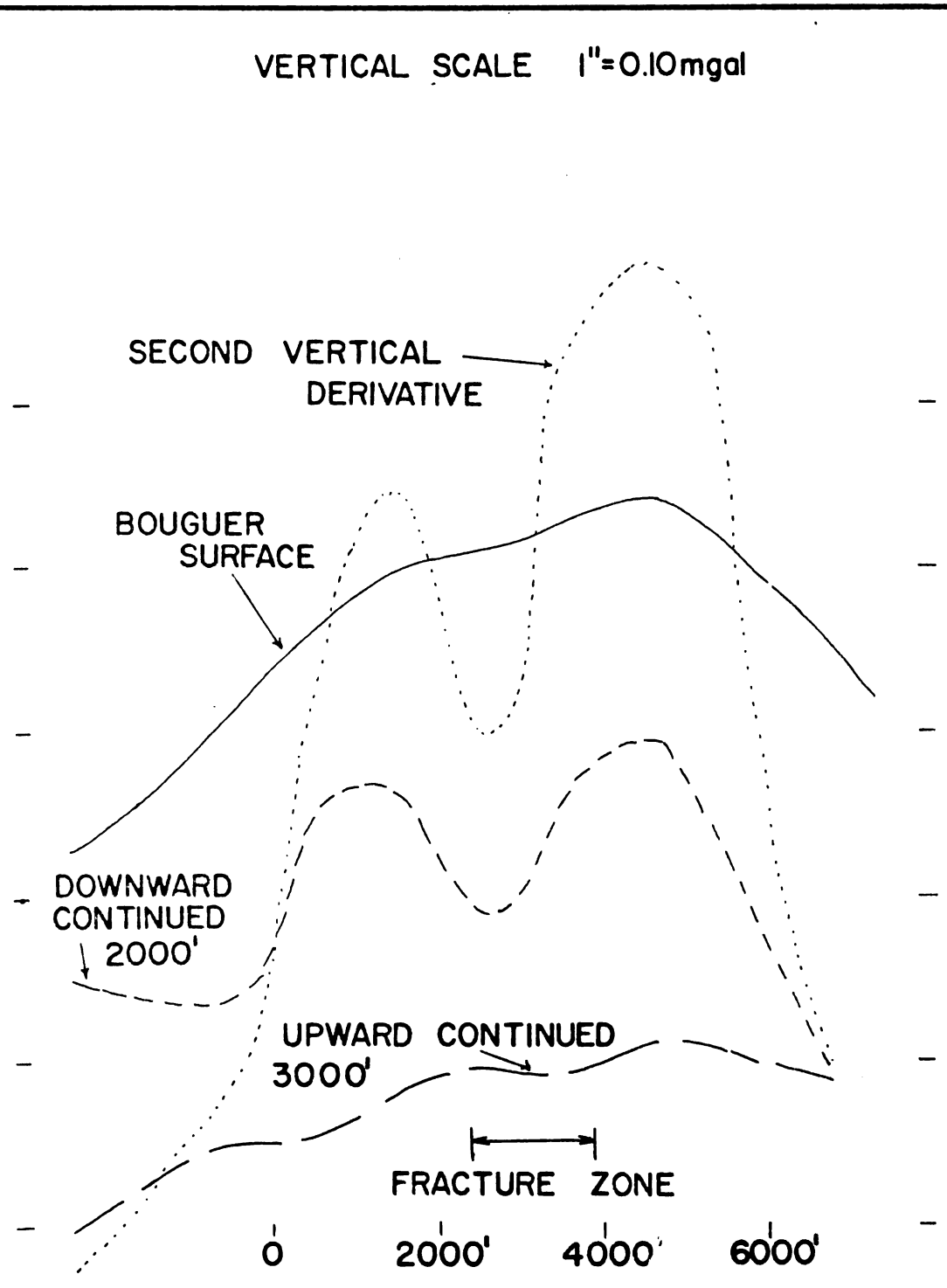

PROFILES OF ANALYTICAL METHODS OVER THE NORTH ADAMS FRACTURE ZONE

FIGURE 20

These profiles, although of only limited extent, indicate that these analytical techniques do not enhance the detection or isolation of the anomalies associated with the fracture zones.

CHAPTER IX

CONCLUSIONS AND RECOMMENDATIONS FOR FURTHER STUDY

Conclusions

The North Adams fracture zone produces a positive anomaly of over 0.10 mgals and is detected by the methods employed in this study. The Deep River fracture zone, although it is longer and broader than the North Adams fracture zone, does not have a detectable anomaly associated with it. It is felt that this is due to the increased porosity of this zone over that of the North Adams fracture zone. Theoretical calculations indicate that the Pinconning fracture zone does not have an anomaly of detectable magnitude associated with it.

There is no relation between the Bouguer gravity anomaly or the least squares residual gravity with the regional geological structures of the area.

Recommendations for Further Study

It is recommended that a greater station density be used over and adjacent to the fracture zones. This would eliminate having to interpolate gravity values in areas of sparse geophysical control. It is also strongly recommended that various combinations of downward continuing upward

continued gravity surfaces be studied to see if these methods enhance or isolate the anomalies due to fracture zones.

BIBLIOGRAPHY

BIBLIOGRAPHY

Cohee, George V., and Landes, Kenneth K. (1958) Oil in the Michigan Basin, in Habitat of Oil, a symposium, A.A.P.G., p. 473-494.

Enlers, G. M., and Radabaugh, R. W. (1938) The Rogers City Limestone, a new Devonian formation in Michigan: Papers of the Mich. Acad. of Science, Arts and Letters, vol. 23, p. 441-446.

Goldich, Samual S., and Parmelee, E. Bruce. (1947) Physical and chemical properties of Ellenburger rocks, Llano County, Texas: Bull., A.A.P.G., vol. 31,pp. 1982-2020.

Henderson, R. G. (1960) A comprehensive system of automatic computation in magnetic and gravity interpretation: Geophysics, vol. 25, no. 3, p. 569-585.

Hinze, W. J. (1963) Regional gravity and magnetic maps of the Southern Peninsula of Michigan: Michigan Dept. of Conservation, Geological Survey Division, Report of Investigation 1.

Hubbert, M. K. (1948) Gravitation terrain effects of two-dimensional topographic features: Geophysics, vol. 13, no. 2, pp. 226-254.

Klasner, J. S. (1964) A study of buried bedrock valleys near South Haven, Michigan by the gravity method: Masters Thesis, Michigan State University.

Landes, K. K. (146) Porosity through dolomitization: Bull., A.A.P.G., Vol. 30, p. 305.

Landes, K. K. (1956) Petroleum Geology: John Wiley and Sons, Inc., New York, pp. 298-301.

Lockett, J. R. (1947) Development of structures in basin areas of Northeastern United States, Bull., A.A.P.G., Vol. 31, pp. 441-443.

Martin, Helen M. (1936) Geological map of the Southern Peninsula of Michigan: Michigan Geol. Survey Pub. 39, geol. ser. 33, Ann. Rept.

Nettleton, L. L. (1940) Geophysical Prospecting for Oil: McGraw-Hill, New York.

Newcombe, R. B. (1933) Oil and gas development in Michigan: Mich. Geol. Survey Pub. 37, Series 31.

Pirtle, G. W. (132) Michigan structural basin and its relationship to surrounding areas: Bull., A.A.P.G., vol. 16, pp. 145-152.

Servos, Gary Gordon (1965) A gravitational investigation of Niagaran reefs in southeastern Michigan: PhD. Thesis, Michigan State University.

Skeels, D. C. (1947) Ambiguity in gravity interpretation: Geophysics, vol. 12, pp. 43-56.

Talwani, M., Worzel, J. Lamer, and Landisman, M. (1959) Rapid gravity computations for two-dimensional bodies with application to the Mendocino submarine fracture zone: Jour. Geophys. Res., Vol. 64, pp. 49-59.

Ver Wiebe, W. A. (1952) North American Petroleum: Edwards Brothers, Inc., Ann Arbor, Michigan, pp. 58-72.

APPENDIX

The following is a list of wells from the Deep River and Pinconning areas that were used in this study. Their locations and permit numbers are given. They are listed according to Township, Range and section number. The wells have been divided into two groups, those of the Deep River area and those of the Pinconning area.

Deep River Area

Township 18 north, Range 3 east

Location	Section	Permit No.
NW¼ NW¼ NW¼	1	13470
SE¼ SW¼ SW¼	1	16382
C SW¼ NE¼	1	10176
NW¼ SW¼ NW¼	1	14868
NW¼ SW¼ SW¼	1	16203
NW¼ NW¼ NE¼	1	15444
SW¼ SW¼ SW¼	1	16052
SE¼ NW¼ SE¼	2	16303
NW¼ NE¼ NE¼	2	15328
NW¼ NW¼ NE¼	2	15627
SE¼ SE¼ SE¼	2	15833
SE¼ NE¼ NE¼	2	14867
NW¼ NE¼ SE¼	2	15135
SW¼ SE¼ SW¼	2	8786
SE¼ SE¼ NE¼	2	2670
SW¼ SW¼ NW¼	12	3123
NW¼ NW¼ NW¼	12	16098
NE¼ NW¼ NW¼	12	16302
NW¼ NE¼ NW¼	12	16383
C SW¼ NE¼	21	1126

Township 18 north, Range 3 east

SE¼ SE¼ SW¼	1	16997
NE¼ NE¼ SE¼	1	16342
SW¼ SW¼ SW¼	1	17273
NW¼ NE¼ SW¼	1	16502
SW¼ SW¼ NE¼	3	14679
SE¼ NE¼ SE¼	4	17867
SE¼ SE¼ NW¼	4	16537

Location	Section	Permit No.
NE¼ SW¼ NE¼	6	5347
NW¼ NW¼ NW¼	6	15535
NW¼ NE¼ NE¼	7	15454
E½ NE¼ SE¼	8	9302
NE¼ SE¼ NW¼	9	8684
NE¼ SE¼ SE¼	9	9032
SE¼ SE¼ NE¼	10	13859
N½ SW¼ SE¼	10	21460
SE¼ NW¼ NE¼	10	14251
SE¼ NW¼ NE¼	10	14212
N½ NE¼ NE¼	10	21239
SE¼ NE¼ SW¼	11	14199
SW¼ SE¼ NE¼	12	16659
NW¼ NW¼ SE¼	13	10770
SE¼ NW¼ SW¼	14	16478
NW¼ NW¼ NW¼	14	13718
SE¼ NE¼ NW¼	16	10421
S½ NE¼ SW¼	16	8000
NW¼ NW¼ NW¼	16	6796
NE¼ SE¼ NW¼	17	13706
SW¼ SE¼ NE¼	18	19720
NW¼ NW¼ NW¼	19	16354
C NW¼ NE¼	19	10285
SE¼ NE¼ SE¼	20	18544
NW¼ NW¼ SW¼	22	13242
S½ SE¼ SE¼	23	16891
NE¼ NE¼ SW¼	24	18724
NW¼ NW¼ NE¼	25	15735
SW¼ SW¼ SW¼	26	18567
C NE¼ SE¼	28	3859
NW¼ SW¼ NW¼	29	12052
NW¼ NW¼ SE¼	29	16860
SW¼ SW¼ SE¼	31	14406
NE¼ NW¼ SE¼	31	18812
NW¼ SE¼ NW¼	31	20490
[illegible] SW¼ NW¼	32	22233
NW¼ NE¼ SE¼	33	15810
SW¼ NW¼ NW¼	36	13579

Township 18 north, Range 5 east

C NW¼ NE¼	5	9733
NE¼ NE¼ SE¼	6	22590
NE¼ NE¼ SE¼	6	21817
NW¼ NW¼ SW¼	9	10934
NE¼ SE¼ SE¼	17	16839
NE¼ NW¼ SW¼	18	12465
NE¼ SE¼ NE¼	19	15021
NE¼ SE¼ SW¼	20	16501
SW¼ NW¼ NW¼	30	17956

Township 19 north, Range 3 east

Location	Section	Permit No.
SE¼ NE¼ NW¼	1	11073
NW¼ SW¼ NW¼	1	12879
SE¼ NE¼ NE¼	2	4203
NW¼ SW¼ NW¼	2	10628
NE¼ NE¼ SE¼	2	14484
NW¼ SW¼ NE¼	3	25102
SE¼ SE¼ NW¼	9	8666
SW¼ SW¼ NE¼	10	13655
NE¼ NE¼ SW¼	11	12702
NE¼ SE¼ SW¼	11	12022
SE¼ NE¼ SW¼	11	12219
SW¼ NW¼ SE¼	11	12327
NW¼ NW¼ SE¼	11	12328
SW¼ SW¼ NE¼	11	12695
SE¼ SE¼ SW¼	11	11819
SE¼ SW¼ NE¼	11	18810
NW¼ SW¼ SE¼	11	11343
SW¼ NE¼ NE¼	11	11249
SW¼ NE¼ NW¼	12	14837
C SW¼ SW¼	13	9711
NW¼ NW¼ NE¼	14	11318
SW¼ SW¼ SW¼	14	7880
NE¼ NW¼ SW¼	14	10702
NW¼ SW¼ SW¼	14	10198
SW¼ NE¼ NW¼	14	11115
SW¼ SE¼ NW¼	14	10821
NW¼ NE¼ NW¼	14	11685
NW¼ SE¼ NW¼	14	10987
SE¼ SW¼ NW¼	14	10774
SE¼ NW¼ NW¼	14	11036
NW¼ SE¼ NW¼	14	10765
NW¼ SW¼ NE¼	14	10855
SW¼ SW¼ NW¼	14	10572
NW¼ SE¼ SE¼	14	11304
NE¼ SE¼ SE¼	15	10497
SE¼ SE¼ SW¼	15	7872
SW¼ SE¼ SE¼	15	8988
SE¼ SE¼ SE¼	15	9158
SE¼ NE¼ SE¼	15	12408
SW¼ SW¼ SE¼	22	10548
NW¼ SW¼ SE¼	22	8773
NE¼ NE¼ NE¼	22	8880
NE¼ SE¼ SW¼	22	8949
SE¼ NE¼ NW¼	22	8382
NE¼ SW¼ SW¼	22	10671
SW¼ NW¼ SE¼	22	9009
NW¼ SE¼ NE¼	22	7895
SE¼ SE¼ NW¼	22	8560
NW¼ SW¼ NE¼	22	8087

Location	Section	Permit No.
SE¼ NW¼ NE¼	22	7907
SW¼ NE¼ NE¼	22	7908
NW¼ NW¼ SE¼	22	8300
NE¼ SW¼ SE¼	22	9008
SE¼ SE¼ SW¼	22	10549
NE¼ SW¼ NW¼	22	9821
NW¼ SE¼ SE¼	22	9289
SW¼ SW¼ NE¼	22	8461
NE¼ NW¼ NE¼	22	9294
SE¼ NE¼ SW¼	22	9169
SE¼ NE¼ NE¼	22	9290
NE¼ NW¼ SE¼	22	8472
SE¼ SW¼ NE¼	22	8345
NE¼ SE¼ NW¼	22	8043
SE¼ NW¼ SE¼	22	9207
NW¼ SW¼ NW¼	23	8480
SW¼ SE¼ SE¼	23	7837
SE¼ SE¼ SW¼	23	7876
SW¼ NW¼ NW¼	23	7875
SE¼ SE¼ SE¼	23	8574
SE¼ SW¼ SE¼	23	8215
NW¼ SE¼ SE¼	23	8192
SW¼ SW¼ SE¼	23	227
NW¼ NW¼ NW¼	23	9214
SW¼ NW¼ NE¼	23	7924
SE¼ SW¼ SW¼	24	8576
SW¼ NW¼ SW¼	24	8654
SW¼ SW¼ SW¼	24	8346
SW¼ SE¼ SW¼	24	4804
SW¼ NW¼ SW¼	24	16855
SE¼ NW¼ NE¼	25	5117
SW¼ NE¼ SW¼	25	23496
C NE¼ SE¼	25	9637
SW¼ NW¼ NE¼	25	4755
C SE¼ NW¼	25	9696
NW¼ NW¼ NW¼	25	8335
SW¼ SE¼ NE¼	25	18538
SW¼ SW¼ NW¼	25	16010
NW¼ NW¼ SW¼	25	4365
C SE¼ SE¼	25	9501
SE¼ NE¼ NW¼	26	4901
C SW¼ SE¼	26	20124
NW¼ NW¼ SE¼	26	4387
NE¼ NW¼ NE¼	26	13373
NW¼ NE¼ NE¼	26	8246
SW¼ NE¼ NW¼	26	13122
SE¼ SW¼ NE¼	26	4855
SE¼ SE¼ NE¼	26	4787
SW¼ NE¼ NE¼	26	4718
NE¼ NE¼ SW¼	26	4508

Location	Section	Permit No.
NE¼ SE¼ SE¼	26	4496
SW¼ NW¼ NE¼	26	5523
NW¼ SE¼ NE¼	26	5160
SE¼ NE¼ SE¼	26	4190
NE¼ NE¼ NW¼	26	6465
NE¼ NE¼ NE¼	26	9102
NE¼ NW¼ SE¼	26	8911
SW¼ SE¼ NE¼	26	14966
C¼ SE¼ SE¼	26	9565
SE¼ NE¼ NE¼	26	15729
NE¼ SE¼ NE¼	26	15236
C NW¼ SE¼	27	9701
NE¼ NE¼ NW¼	27	9377
SW¼ SW¼ SE¼	27	17314
C SE¼ NW¼	27	9844
S½ NE¼ NW¼	27	10547
C SE¼ SW¼	28	10390
NW¼ SW¼ NW¼	34	24207
SE¼ SE¼ SE¼	34	15429
SE¼ SW¼ NE¼	34	16669
SE¼ SE¼ NE¼	34	16300
NW¼ SW¼ SE¼	35	15654
C SE¼ NW¼	35	9705
SW¼ NW¼ NE¼	35	15311
SW¼ SW¼ NE¼	35	15691
SE¼ NE¼ SW¼	35	15521
NE¼ NE¼ SW¼	35	15690
SE¼ SE¼ SW¼	35	15321
SE¼ NW¼ SW¼	35	15610
NW¼ NW¼ SE¼	35	15605
SE¼ SW¼ NW¼	35	16798
NW¼ NW¼ SW¼	35	15857
SE¼ NW¼ SE¼	35	16301
C NE¼ SE¼	35	9520
SE¼ SE¼ NE¼	35	12847
NW¼ SE¼ SW¼	35	15842
NE¼ NE¼ NE¼	35	4618
SE¼ SE¼ SE¼	35	15222
SW¼ NW¼ NW¼	35	16746
SE¼ SW¼ SE¼	35	15218
NE¼ SE¼ SE¼	35	13705
SE¼ SE¼ NW¼	36	15622
SE¼ SW¼ SW¼	36	14885
C SW¼ SW¼	36	9638
C SE¼ NE¼	36	9636
C NW¼ NE¼	36	9500
SE¼ NE¼ NE¼	36	18593
SE¼ SE¼ SW¼	36	15590
NE¼ SW¼ SW¼	36	15574

Location	Section	Permit No.
C SE¼ SW¼	36	10056
N½ NW¼ SW¼	36	16686
SE¼ NW¼ SW¼	36	15614
NE¼ NE¼ NE¼	36	9293
N½ NE¼ NE¼	36	21855

Township 19 north, Range 4 east

SE¼ NW¼ SW¼	1	21256
S½ SW¼ SW¼	5	10593
S½ SW¼ SE¼	6	10662
SE¼ SW¼ SE¼	6	10960
SE¼ SW¼ NE¼	6	11248
SE¼ NE¼ SW¼	6	11498
SW¼ SE¼ SE¼	6	11576
NE¼ SE¼ SW¼	6	13541
NE¼ NE¼ SW¼	6	11268
SE¼ SE¼ SE¼	6	11292
SE¼ SE¼ NE¼	7	10869
NE¼ SE¼ NE¼	7	11450
SW¼ SW¼ SW¼	7	11787
NE¼ NE¼ NE¼	7	12340
C SW¼	7	10331
S½ NE¼ NE¼	7	10617
S½ NW¼ NE¼	7	10672
NW¼ NE¼ NE¼	7	11387
NE¼ NW¼ NE¼	7	11285
SE¼ SE¼ SE¼	7	17649
NE¼ NE¼ SW¼	8	11071
SE¼ NE¼ SE¼	8	11107
NW¼ SW¼ NW¼	8	11577
S½ SE¼ SE¼	8	9506
SE¼ SW¼ NW¼	8	10620
S½ NW¼ NW¼	8	10433
SW¼ SE¼ NE¼	8	11578
NE¼ NW¼ SE¼	8	11358
NE¼ NE¼ SE¼	8	11357
NE¼ SE¼ NW¼	8	11226
NE¼ SW¼ NW¼	8	11448
NW¼ NW¼ SE¼	8	10925
NW¼ SW¼ NE¼	8	10839
NE¼ NW¼ NW¼	8	12619
NW¼ NW¼ NW¼	8	12339
SW¼ SE¼ NW¼	8	12178
SW¼ SW¼ NE¼	8	11842
NE¼ SW¼ NE¼	8	11958
SE¼ SW¼ NE¼	8	10691
SW¼ NE¼ NW¼	8	11575
NE¼ SW¼ SW¼	9	11841

Location	Section	Permit No.
SW¼ SW¼ SW¼	9	12809
NW¼ NW¼ SW¼	9	10924
SW¼ SE¼ SW¼	9	11843
SW¼ SE¼ SE¼	9	11383
SE¼ NW¼ SW¼	9	11157
SE¼ SW¼ SW¼	9	10965
NW¼ SW¼ SW¼	9	11109
SW¼ NW¼ SW¼	9	11838
SE¼ SE¼ SW¼	9	11232
SW¼ SW¼ SE¼	9	11259
SW¼ NW¼ NW¼	9	11451
SE¼ NE¼ SW¼	9	11233
NW¼ NW¼ SE¼	9	11042
E½ NE¼ SE¼	9	8476
SW¼ NW¼ NE¼	9	11373
NW¼ SW¼ NW¼	10	10867
NW¼ NE¼ SW¼	14	11874
SW¼ SE¼ SW¼	14	12029
SW¼ SW¼ NW¼	14	11753
SE¼ SE¼ SW¼	14	12030
SW¼ SW¼ SW¼	14	19748
SE¼ SW¼ SW¼	14	12038
SW¼ SW¼ SE¼	14	11951
SW¼ NW¼ SE¼	14	20155
SE¼ SW¼ SE¼	14	12134
NW¼ SW¼ SW¼	14	11952
SW¼ SW¼ SW¼	15	19299
SE¼ SW¼ SE¼	15	11989
SW¼ SE¼ SE¼	15	12276
SE¼ NE¼ SW¼	15	11872
SE¼ NE¼ SE¼	15	12689
NE¼ SW¼ NW¼	15	12062
SW¼ SW¼ NW¼	15	11956
NE¼ SE¼ SE¼	15	11884
SW¼ NE¼ SW¼	15	12037
NW¼ SW¼ SE¼	15	11997
SW¼ NE¼ SW¼	15	11619
NW¼ NE¼ SW¼	15	11613
SW¼ NW¼ NW¼	15	11502
SE¼ SW¼ NW¼	15	11500
NW¼ SW¼ NW¼	15	11379
NW¼ SE¼ SE¼	15	11782
SE¼ NW¼ SE¼	15	11754
NE¼ NE¼ SW¼	15	11715
SW¼ NW¼ SE¼	15	11708
SW¼ SE¼ NW¼	15	11641
NE¼ NW¼ SW¼	15	11640
SE¼ SE¼ NW¼	15	11907
NE¼ SE¼ SW¼	15	12061

Location	Section	Permit No.
SE¼ NW¼ NW¼	15	12147
NW¼ NW¼ NW¼	15	11342
NW¼ NW¼ SW¼	15	11262
SW¼ SW¼ SE¼	15	20235
SW¼ NW¼ SW¼	15	19657
NW¼ NE¼ NW¼	16	10956
NW¼ SE¼ NW¼	16	10974
SW¼ SW¼ SW¼	16	14693
SW¼ NE¼ SE¼	16	3619
SW¼ SE¼ NE¼	16	12148
SE¼ NW¼ NW¼	16	14398
SW¼ SW¼ SE¼	16	18293
SW¼ NE¼ SW¼	16	19612
SE¼ SE¼ NE¼	16	11871
SW¼ NE¼ NE¼	16	11924
SW¼ NW¼ NE¼	16	12003
NE¼ NE¼ NE¼	16	12002
SE¼ NE¼ NE¼	16	11536
NE¼ SE¼ NE¼	16	11501
NW¼ SE¼ NE¼	16	11426
NW¼ NE¼ NE¼	16	11382
NE¼ NE¼ NW¼	16	11374
SE¼ NW¼ NE¼	16	11261
NW¼ NW¼ NE¼	16	11118
SE¼ SW¼ SW¼	17	14517
NW¼ NW¼ SW¼	17	13866
NE¼ SE¼ SE¼	17	16133
NW¼ SW¼ SW¼	17	13812
SW¼ SW¼ SE¼	17	14547
SW¼ NW¼ NW¼	17	15971
C SE¼	18	10280
C NE¼	18	10216
NE¼ SE¼ SE¼	18	13728
SE¼ NE¼ SE¼	18	13665
SW¼ SE¼ NE¼	18	14108
NE¼ SE¼ NE¼	18	14386
SE¼ NE¼ NE¼	18	15730
NW¼ SE¼ NE¼	18	14387
NW¼ SE¼ SE¼	18	13771
SW¼ NE¼ NE¼	18	14450
NE¼ NE¼ SE¼	18	13764
NW¼ NE¼ SE¼	18	14109
SW¼ NE¼ SE¼	18	13776
SE¼ SE¼ SE¼	18	19705
SE¼ NE¼ NE¼	20	17439
NW¼ NE¼ NW¼	20	16996
NW¼ NE¼ SE¼	20	14805
SW¼ NE¼ NE¼	20	20349
SE¼ SW¼ NW¼	20	19463

Location	Section	Permit No.
SW¼ SW¼ NW¼	21	19557
SW¼ NW¼ NE¼	21	19353
SW¼ NE¼ NW¼	21	19615
SW¼ NW¼ NW¼	21	17632
SW¼ NW¼ NW¼	21	18705
SW¼ NE¼ NE¼	21	19030
SW¼ NW¼ SW¼	22	19536
SW¼ NE¼ NE¼	22	19476
SW¼ SE¼ NW¼	22	19354
SW¼ NW¼ NW¼	22	19171
SW¼ SW¼ NE¼	22	19623
NW¼ NE¼ NW¼	22	11243
NE¼ SW¼ NE¼	23	16594
NW¼ NE¼ NE¼	23	12073
NW¼ NW¼ NE¼	23	11894
NE¼ SE¼ NW¼	23	12563
NW¼ NE¼ NW¼	23	12060
NE¼ NW¼ NE¼	23	11970
SE¼ SE¼ NE¼	23	12204
SE¼ NE¼ NW¼	23	12403
SW¼ NW¼ NE¼	23	12342
SW¼ NE¼ NW¼	23	12479
SW¼ NW¼ SE¼	23	18524
SW¼ SE¼ NW¼	23	19903
NW¼ NW¼ SE¼	23	11531
SE¼ SE¼ NW¼	24	12398
NW¼ NW¼ SW¼	24	12090
NE¼ NE¼ SW¼	24	17186
W½ SE¼ NW¼	24	13755
NW¼ SW¼ NW¼	24	12146
SW¼ SW¼ NW¼	24	12300
SW¼ NE¼ NW¼	24	12120
SE¼ NW¼ NW¼	24	12133
SW¼ NW¼ NW¼	25	11620
SE¼ NE¼ NE¼	25	14010
SW¼ NE¼ NW¼	25	19973
SW¼ NW¼ NE¼	26	23799
NE¼ SE¼ SW¼	27	2412
NW¼ SW¼ NE¼	27	11781
NE¼ SW¼ NW¼	27	10984
NW¼ NW¼ SW¼	27	16924
SW¼ NE¼ NW¼	28	17341
NE¼ SW¼ SW¼	28	11847
NE¼ NE¼ NW¼	29	14772
SE¼ SW¼ NW¼	29	21465
NW¼ SW¼ NE¼	29	11988
C NW¼ NW¼	31	9502
NE¼ NW¼ SE¼	32	4094
SE¼ NW¼ SW¼	36	9288

Township 19 north, Range 5 east

Location	Section	Permit No.
SE¼ NE¼ SW¼	8	4905
SE¼ SE¼ NW¼	10	4391
SW¼ SW¼ SE¼	17	11812
NW¼ SW¼ SW¼	19	12878
NW¼ NW¼ NW¼	29	5971
NE¼ NW¼ NW¼	30	11906
SE¼ NE¼ SW¼	31	19172
NW¼ SW¼ SW¼	32	21232

Pinconning Area

Township 15 north, Range 4 east

SE¼ SW¼ NW¼	10	2054
SW¼ SW¼ NE¼	20	8403

Township 16 north, Range 3 east

NW¼ NW¼ NW¼	23	16140
SW¼ SW¼ SW¼	35	3247

Township 16 north, Range 4 east

NW¼ NW¼ SW¼	2	14747
NE¼ SW¼ NW¼	2	12152
NW¼ SW¼ NW¼	2	11966
NE¼ NW¼ NW¼	2	14501
NW¼ NW¼ NE¼	2	13745
NW¼ SW¼ NE¼	2	12740
NW¼ SE¼ NW¼	2	12214
SW¼ SW¼ NE¼	2	12177
SW¼ SE¼ NW¼	2	11192
SW¼ NW¼ NE¼	2	11315
SW¼ NE¼ NW¼	2	10944
SW¼ NE¼ SE¼	2	13885
SW¼ NW¼ SW¼	2	11138

Township 16 north, Range 5 east

NW¼ NW¼ SW¼	7	4613

Township 17 north, Range 5 east

E½ SW¼ NE¼	13	16608
SW¼ SE¼ SE¼	13	12963
SW¼ SE¼ NE¼	13	13509
SW¼ SW¼ SE¼	13	13342
SW¼ NE¼ SE¼	13	13367

Location	Section	Permit No.
NE¼ SE¼ SE¼	13	15140
NE¼ NE¼ SE¼	13	15203
NE¼ SW¼ NE¼	24	13915
NE¼ NE¼ NW¼	24	13853
NE¼ NW¼ SE¼	24	14152
SW¼ NE¼ NE¼	24	13795
NE¼ SE¼ NE¼	24	14602
NE¼ NE¼ SE¼	24	14858
NE¼ NE¼ NE¼	24	15044

Township 17 north, Range 4 east

SW¼ NW¼ NE¼	12	3690
SE¼ SE¼ NE¼	16	12455
NW¼ NE¼ NW¼	17	2107
SW¼ SE¼ NW¼	18	13338
SW¼ NW¼ SW¼	18	13596
SW¼ SW¼ SE¼	18	13658
SW¼ SW¼ NE¼	18	13692
SW¼ SW¼ NW¼	18	13491
SW¼ SE¼ SW¼	18	13138
NE¼ SW¼ SW¼	18	13436
SW¼ SW¼ SW¼	18	13365
SW¼ NE¼ SW¼	18	13539
NE¼ NE¼ SE¼	18	18024
NE¼ SE¼ SW¼	18	17429
NE¼ NW¼ SE¼	18	17930
NE¼ NW¼ SW¼	18	17326
SW¼ NW¼ NE¼	18	14070
NE¼ SW¼ SE¼	18	17510
NE¼ SE¼ SE¼	18	17704
SE¼ NE¼ SW¼	18	17720
NE¼ SE¼ NE¼	18	18101
SW¼ NE¼ NW¼	19	13353
SW¼ NW¼ NW¼	19	14117
SW¼ SW¼ NW¼	19	14761
SW¼ SE¼ SW¼	21	13737
SW¼ NW¼ SE¼	25	11193
NE¼ NW¼ SE¼	25	17093
SE¼ SW¼ SW¼	25	17496
NE¼ NE¼ SW¼	25	20946
NE¼ SW¼ SW¼	25	17304
NE¼ NE¼ SW¼	25	17728
NW¼ SW¼ NE¼	25	17465
NE¼ NW¼ SW¼	25	17866
NW¼ NW¼ SE¼	25	18377
SW¼ NE¼ SW¼	25	17595
SE¼ SW¼ SW¼	27	2749

Location	Section	Permit No.
NW¼ NE¼ NW¼	29	16510
NE¼ SW¼ NE¼	29	15297
SE¼ NW¼ NE¼	29	16178
NE¼ NE¼ NE¼	29	16585
SW¼ NE¼ NE¼	29	16398
SW¼ SW¼ NE¼	29	15220
SW¼ SE¼ NE¼	29	15970
SW¼ NW¼ NE¼	30	14859
SW¼ SE¼ NE¼	33	15708
SW¼ SE¼ SW¼	34	11106
SW¼ NE¼ SW¼	35	11158
SW¼ SW¼ SE¼	35	13578
SW¼ SE¼ NE¼	35	13809
SW¼ NW¼ SW¼	35	12224
SE¼ NW¼ SE¼	35	13969
SE¼ SW¼ SE¼	35	13811
SE¼ SE¼ SW¼	35	12213
NE¼ SE¼ NE¼	35	13919
NE¼ NE¼ NE¼	35	12615
SE¼ SE¼ SW¼	35	12860
NW¼ NE¼ SE¼	35	13951
NW¼ SW¼ NW¼	36	16954
SW¼ NW¼ NW¼	36	14228
NE¼ NE¼ NW¼	6	21882
NE¼ NW¼ NW¼	32	13838